

Closed-Form Expressions for Nonlinearity Coefficients in Multimode Fibers

Paolo Carniello, Filipe M. Ferreira, *Senior Member, IEEE*, Norbert Hanik *Senior Member, IEEE*

Abstract—We derive novel approximate closed-form expressions for the nonlinear coupling coefficients appearing in the Manakov equations for multimode fibers for space-division multiplexing in the two regimes of strong and weak coupling. The expressions depend only on few fiber design parameters. In particular, the Manakov coefficients are shown to be simple rational numbers which depend solely on the number of guided modes. The overall nonlinearity coefficients are found to decrease with increasing core radius and to stay nearly constant with increasing refractive index difference between core and cladding. Validation is performed through a numerical approach. The consequences of the findings onto fiber design are discussed in terms of achievable data rates. The analysis is mainly focused on the trenchless parabolic graded-index profile, but considerations on the use of realistic trenches and non-parabolic indices, and on the step-index profile are given.

Index Terms—Multimode fibers, space division multiplexing, Manakov equations, nonlinear coupling coefficients, optical communications.

I. INTRODUCTION

IN the field of space-division multiplexing (SDM) the most common fiber structures are multicore fibers (MCFs) and multimode fibers (MMFs). Based on the level of linear coupling among the fiber modes, two common operational regimes are distinguished: the weak coupling regime (WCR) and the strong coupling regime (SCR) [1]. In the WCR, modes belonging to the same mode group are assumed to be strongly-coupled, while modes of different groups are assumed to be uncoupled, as for MMFs with sufficient phase-mismatch among the mode groups as well as for weakly-coupled MCFs (WC-MCFs) [2]. In the SCR, all fiber modes are assumed to be strongly coupled, as for randomly-coupled MCFs (RC-MCFs) [3], and for graded-index multimode fibers (GIMMFs) with suitable techniques to enhance coupling – e.g., using long period fiber gratings [4], [5], [6]. In long-haul communications it is often tried to achieve the SCR such that delay spread and mode-dependent loss (MDL) accumulate at a slower pace with transmission distance (e.g., ideally with the square-root of distance), compared to the case of partial coupling [7], [8], [9]. The level of coupling can be directly controlled in MCFs through, e.g., the separation of

the cores [10], [11], while it is generally less straightforward to be tuned in MMFs. Hence, MCFs are considered to be the preferred medium for long-haul communications given their potential for smaller digital signal processing (DSP) complexity thanks to a generally lower delay spread, when compared to MMFs with the same number of modes [12], [3], [10].

In addition, MMF-based SDM systems tend to have a stronger frequency-dependence in the delay spread, higher mode-averaged attenuation and MDL, due to stronger Rayleigh scattering (because of the core’s doping) [1], [12], [13].

However, several MMF system architectures have been under investigation to reduce the delay spread, from optimized fiber designs [13], [14], to the introduction of intentional coupling through, e.g., spinning during the manufacturing process [15], to the use of gratings as mode couplers [4], [5], [6] or of cyclic modal permutation [5], [16], or fiber spans with different sign of modal delay [5], [1]. More importantly, MMFs can potentially achieve a higher spatial-spectral efficiency than that of MCFs, given their ability to support a larger number of spatial paths [13], [17] in the same cross-sectional area of a single mode fiber (SMF), even above 1000, which had been speculated to be potentially needed by 2035 [18]. This is a strong motivation for investigating MMFs for long distances and, thus, for bringing into play the Kerr nonlinear response of silica fibers.

Kerr nonlinearity depends on the matrix of nonlinear coupling coefficients $\gamma\kappa$, which in the SCR reduces to the scalar $\gamma\kappa$ which is sometimes assumed to scale as $1/M$, where M is the total number of modes [19]. In such a case, under certain conditions, spectral efficiency per mode would increase with M [19]. However, as we showed in [20], the $1/M$ scaling of $\gamma\kappa$ is valid only for a particular fiber design strategy, that is by increasing only the core radius.

In this paper we extend the study of [20] by providing analytic derivations of approximate closed-form expressions for the nonlinearity coefficients γ , κ , and $\gamma\kappa$ for the SCR, and for κ and $\gamma\kappa$ for the WCR, for different GIMMF design approaches. The closed-form results clarify the relation between the nonlinearity coefficients and the fiber design parameters. In particular, we found that the elements of κ are simple rational numbers which depend only on M . As γ depends on the effective area \mathcal{A}_{11} of the fundamental mode, the elements of $\gamma\kappa$ are shown to depend only on \mathcal{A}_{11} , once M is fixed. Maximizing \mathcal{A}_{11} minimizes the elements of $\gamma\kappa$. In particular, they decrease with increasing core radius R and stay nearly constant with increasing refractive index difference between core and cladding Δ .

The derived closed-form expressions require significantly lower computational time than the current numerical approach.

The work of Paolo Carniello was financially supported by the Federal Ministry of Education and Research of Germany in the program of “Souverän. Digital. Vernetzt.”. Joint project 6G-life, project identification number: 16KISK002. The work of Filipe M. Ferreira was financially supported by a UKRI Future Leaders Fellowship [grant numbers MR/T041218/1 and MR/Y034260/1].

Paolo Carniello and Norbert Hanik are with the Institute for Communications Engineering, Technische Universität München, Germany (email: paolo.carniello@tum.de).

Filipe M. Ferreira is with the Optical Networks Group, Dept. Electronic and Electrical Eng., University College London, U.K..

For example, in the case of a 2352-modes MMF, the computation of the modal profiles with a mode solver required us ~ 4.5 hours on a server equipped with two 16-cores AMD EPYC 7282 processors at 3.2 GHz (even though no parallel workers are used in our MATLAB implementation) and 256 GB of RAM. From the modal profiles, the computation of $\gamma\kappa$ from their definition required ~ 2 hours on a server equipped with a 32-cores AMD EPYC 7543P processor at 2.8 GHz (only 4 workers could be used in our MATLAB implementation not to exceed the RAM limit) and 512 GB of RAM. On the opposite, the closed-form expressions derived here can be computed almost instantaneously. Additionally, they free researchers who deal with, e.g., the development of models for the nonlinear SDM channel like in [21], [22], [23], from the task of choosing a specific fiber design and computing (or assuming) some values for $\gamma\kappa$. Although the analytic formulas we derive hold formally only for a trenchless GIMMF with parabolic grading, some considerations about the validity of the present results for more general fiber designs are provided in Section V, and about the step-index profile in Section IV.

The paper is organized as follows. Section II reviews the channel models for the SCR and WCR. Section III reviews the basics of fiber design. Section IV presents the main numerical and analytic results about the nonlinear coupling coefficients. In Section V $\gamma\kappa$ values for optimized and manufactured fibers proposed in the literature are computed, showing agreement with our framework. Section VI explains the implication of this study onto fiber design through the achievable data rate in a simple SDM scenario, highlighting that the rate does not increase in general with number of modes, but the scaling rather depends on the fiber design. Section VII collects some side remarks. Section VIII concludes the paper.

II. BASICS OF CHANNEL MODELING

A common nonlinear propagation equation for the SCR is the following Manakov equation [24], [25], [19]

$$\frac{\partial \mathbf{A}}{\partial z} = \mathbf{L}_{\text{SCR}}[\mathbf{A}] - j\gamma\kappa\|\mathbf{A}\|^2\mathbf{A} \quad (1)$$

where $\mathbf{A} = [A_1, \dots, A_M]^T$ is the column vector of modal envelopes (T is the transpose operator), M is the total number of modes (i.e., including polarizations), and $\mathbf{L}_{\text{SCR}}[\mathbf{A}]$ is the linear operator accounting for all linear effects, in particular strong mode-coupling and dispersion. The last term of Eq. (1) is Kerr nonlinear effect, which depends on two coefficients that in the weak-guidance approximation (which is commonly assumed to hold for fibers for modern optical communications [26]) can be computed as [25], [19]

$$\gamma = \frac{\omega_0 n_2}{c\mathcal{A}_{11}} \quad (2)$$

$$\kappa = \frac{4}{3} \frac{2N}{2N+1} \frac{\mathcal{A}_{11}}{N^2} \sum_{a=1}^N \sum_{b=1}^N \frac{1}{\mathcal{A}_{ab}} \quad (3)$$

where N is the number of spatial modes (so that $N = M/2$), and

$$\mathcal{A}_{ab} = \frac{\int_{-\infty}^{\infty} \int_{-\infty}^{\infty} \|\mathbf{F}_a\|^2 dx dy \int_{-\infty}^{\infty} \int_{-\infty}^{\infty} \|\mathbf{F}_b\|^2 dx dy}{\int_{-\infty}^{\infty} \int_{-\infty}^{\infty} \|\mathbf{F}_a\|^2 \|\mathbf{F}_b\|^2 dx dy} \quad (4)$$

is the intermodal effective area between spatial modes \mathbf{F}_a and \mathbf{F}_b [19, Eq. 60]. The working wavelength is $\lambda_0 = 1550$ nm, $\omega_0 = 2\pi c/\lambda_0$ is the working angular frequency, $k_0 = \frac{2\pi}{\lambda_0}$ is the wavenumber in vacuum, the nonlinear refractive index is $n_2 = 2.6 \cdot 10^{-20} \text{ m}^2\text{W}^{-1}$, and c is the light-speed in vacuum.

For the WCR, a common nonlinear propagation equation is the following Manakov equation [27], [19, Eq. 54]

$$\frac{\partial \mathbf{A}_a}{\partial z} = \mathbf{L}_{\text{WCR}}[\mathbf{A}_a] - j\gamma \sum_{b=1}^G \kappa_{ab} \|\mathbf{A}_b\|^2 \mathbf{A}_a \quad (5)$$

where \mathbf{A}_a is the N_a -dimensional vector obtained by stacking only the modal amplitudes of the a -th mode group, N_x is the number of spatial modes of the x -th mode group, G is the total number of mode groups, and this time $\mathbf{L}_{\text{WCR}}[\mathbf{A}_a]$ accounts for the linear effects of the WCR. Note that, conversely to Eq. (1), Eq. (5) contains multiple nonlinear coupling coefficients, which in the weak-guidance can be computed as [19, Eq. 61 - 63]

$$\kappa_{ab} = \frac{4}{3} \frac{2N_a}{2N_a + \delta_{ab}} \frac{\mathcal{A}_{11}}{\bar{\mathcal{A}}_{ab}} \quad (6)$$

where $\delta_{ab} = \begin{cases} 1 & \text{if } a = b \\ 0 & \text{if } a \neq b \end{cases}$ is the Kronecker's delta, and

$$\bar{\mathcal{A}}_{ab} = \left(\frac{1}{2N_a 2N_b} \sum_{\alpha \in I_a} \sum_{\beta \in I_b} \frac{1}{\mathcal{A}_{\alpha\beta}} \right)^{-1} \quad (7)$$

with I_x being the set of indices of the modes (including polarizations) which belong to group x . Note that the various κ_{ab} can be grouped in the matrix κ . In case of a single group of degenerate modes, Eq. (6) reduces to Eq. (3).

For GIMMFs, we consider only fibers supporting $M = G(G+1)$ modes, where G is the total number of mode groups, and each group consists of $M_g = 2g$ (with $g \in \{1, 2, \dots, G\}$) modes (including polarizations), as customary in the literature [28, Sec. 11.2.2]. Then, in the WCR the sizes of the groups are M_g . In the SCR, due to the assumption of strong linear coupling among, all modes can be thought as belonging to a single group of size M .

As a side remark, some MMF systems might not strictly operate in either of the two considered regimes, SCR and WCR, but rather in an intermediate coupling regime [29], [30], [31], whose study is however outside the scope of this paper.

Throughout the paper we present and compare three methods for computing nonlinear coupling coefficients. The first method, which serves as reference approach, consists in numerically computing the modal profiles for the fiber geometry of interest with a mode solver, and then carrying out the numerical integration of Eq. (4) to get κ with Eq. (6). The second method consists in exploiting analytic closed-form expressions for Eq. (2) and Eq. (6) derived later in this work. The third method consists in fitting the results obtained with the first one. In the following we will refer to the first method as the numerical method, to the second as the analytic method, and to the third as the fitted formula.

III. BASICS OF FIBER DESIGN

Designing a MMF essentially consists in selecting the refractive index profile $n(\rho)$ of the fiber, where ρ is the radial coordinate. Common profiles, that are the ones which we consider, are the parabolic graded-index (GI) and the step-index (SI), which are defined respectively as [32, Eq. 2.78]

$$n_{\text{GI}}(\rho) = \begin{cases} n_{\text{core}} \sqrt{1 - 2\Delta \left(\frac{\rho}{R}\right)^2}, & \text{if } \rho \leq R \\ n_{\text{core}} \sqrt{1 - 2\Delta}, & \text{if } \rho > R \end{cases} \quad (8)$$

and

$$n_{\text{SI}}(\rho) = \begin{cases} n_{\text{core}}, & \text{if } \rho \leq R \\ n_{\text{clad}}, & \text{if } \rho > R \end{cases} \quad (9)$$

where $\Delta = (n_{\text{core}}^2 - n_{\text{clad}}^2)/(2n_{\text{core}}^2)$ is the refractive index difference, n_{core} is the maximum value of $n(\rho)$ in the core, n_{clad} is the constant value of $n(\rho)$ in the cladding, and R is the core radius.

In case advanced refractive index profiles (like a non-parabolic graded-index) or trenches were employed, which is not done here, few more geometrical parameters would have to be taken into account. Some considerations about the extension of the presented results to non-parabolic GI profiles with trenches are given in Section V.

The total number of guided modes M depends on $n(\rho)$ and on the normalized frequency $V = k_0 R \text{NA} = k_0 R n_{\text{core}} \sqrt{2\Delta}$, where $\text{NA} = \sqrt{n_{\text{core}}^2 - n_{\text{clad}}^2} = n_{\text{core}} \sqrt{2\Delta}$ is the so-called numerical aperture [32, Eq. 2.80]. For a GIMMF, an approximate relation between V and M is [32, Eq. 2.81]

$$M \approx \frac{V^2}{4} \quad (10)$$

while for a step-index multimode fiber (SIMMF) it holds [32, Eq. 2.61]

$$M \approx \frac{V^2}{2} \quad (11)$$

Observe that, even though M is formally a positive integer, it will be sometimes treated here as a positive real number for simplicity of notation.

The design of a MMF aims at minimizing several detrimental effects like modal delays, MDLs, and coupling losses (in particular bend losses) [33], [34], [13], while guiding a specific number of modes. It is known that increasing Δ tends to increase the modal delays, and the mode-averaged and relative Rayleigh scattering of the different modes, which influence the mode-averaged attenuation and the MDL [13]. However, a higher Δ better confines the modal profiles, reducing the bend losses [35]. Increasing R is a straightforward approach to increase M , but it is hard to support more than approximately 200 modes without increasing Δ (beyond a conventional $\sim 0.5\%$). Hence, it is in general helpful to tune both R and Δ when designing a fiber for a specific M [33], [13]. As such, it is of interest to study the scaling of $\gamma\kappa$ in the general scenario where both R and Δ are varied. Since the present work focuses on the study of the nonlinearity coefficients only, the reader is redirected to the above-referenced papers for a review and assessment of the scaling of the mentioned detrimental linear effects with fiber design parameters. The study of MMF designs

balancing linear and nonlinear effects is outside of the scope of the paper and left for future research, which can benefit from the present work. Some initial glimpses are provided in [36].

For the design of fibers employed later for numerical analysis, we set $n_{\text{clad}} \approx 1.444$, as for a pure silica cladding at 1550 nm. Even though the actual fiber material is not relevant for our single-frequency study, in practice values of $n(\rho)$ higher than n_{clad} (e.g., for the core) can be achieved with germanium doping, while lower values (e.g., for trenches) can be obtained with fluorine doping [37].

Given a fiber supporting M modes, it has always been chosen for the numerical results of this paper the highest possible V before reaching the cutoff frequency V_c of the subsequent mode group, so that the guided modes exhibit the strongest confinement [38], [33], [13].

All numerical results have been obtained with the linearly polarized (LP) mode solver implemented in MATLAB described in [39], based on [40], and valid under the assumption of weak-guidance. For the GIMMFs, a square grid of 600×600 evenly spaced points has been used, covering a square integration area with edge length of $125 \mu\text{m}$ ($50 \mu\text{m}$ for the GIMMFs with $R = R_{\text{GISMF}} = 6.6 \mu\text{m}$). Larger grid sizes have been observed to produce negligible effects on the computation of the quantity of interest, i.e., $\gamma\kappa_{ab}$. For the SIMMFs, a square grid of at least 300×300 evenly spaced points has been used, covering a square integration area with edge length of $125 \mu\text{m}$ ($90 \mu\text{m}$ for the GIMMFs with $R = R_{\text{GISMF}} = 4.1 \mu\text{m}$). Larger grid sizes have been observed to produce negligible effects on the computation of the quantity of interest, i.e., $\gamma\kappa$. The choice of modal basis is irrelevant for $\gamma\kappa$, as long as the modes of a mode group of a certain basis are obtained through a unitary transformation of (quasi-)degenerate vector modes [41], [42]. The cutoff frequencies V_c for the various modes have been computed with the implicit method in [43, Eq. 6] for GIMMFs, and as zeros of Bessel functions of the first-kind for SIMMFs [44, p. 320], assuming weak-guidance in both cases.

IV. SCALING OF THE NONLINEAR COUPLING COEFFICIENTS WITH INDEX DIFFERENCE AND CORE RADIUS

This section presents the main numerical and analytical results of this work about the nonlinear coupling coefficients. We start from the SCR in Section IV-A for which the scalars γ , κ , and $\gamma\kappa$ are examined, followed by the WCR case in Section IV-B for which the matrices κ and $\gamma\kappa$ have to be considered. The analysis is mainly carried out for GIMMFs; some considerations on SIMMFs are provided in Section IV-C.

A. Strong Coupling Regime

In order to understand the scaling of $\gamma\kappa$ in a generic scenario where both R and Δ are varied, we firstly consider cases in which only one of the two parameters is varied, while the other is held fixed. In doing so, we also find bounds on $\gamma\kappa$, as it will be clear later. In particular, we start from a baseline GIMMF with core radius $R = R_{\text{GISMF}}$ and refractive index $\Delta = \Delta_{\text{GISMF}}$. Then, a first design option is to increase only

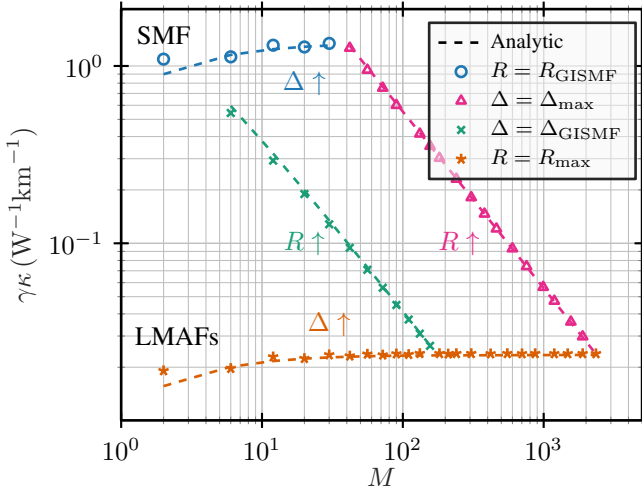


Figure 1: Scaling of $\gamma\kappa$ with M for different GIMMF designs. Markers indicate numerical results with the approach explained in the text. The dashed lines are the proposed theoretical trends: the line relative to the circles is Eq. (16) with $R = R_{\text{GISMF}}$; the line relative to the triangles is Eq. (14) with $\Delta = \Delta_{\text{max}}$; the line relative to the crosses is Eq. (14) with $\Delta = \Delta_{\text{GISMF}}$; the line relative to the stars is Eq. (16) with $R = R_{\text{max}}$. The symbol $R \uparrow$ indicates that only R is increased; $\Delta \uparrow$ indicates that only Δ is increased.

Table I: Parameters for relevant GIMMFs in Fig.1

M	Δ (%)	R (μm)	\mathcal{A}_{11} (μm^2)	κ	$\gamma\kappa$ (1/W/km)
2	0.41	6.6	86	8/9	1.1
2	0.0072	50	4900	8/9	0.019
42	5.0	6.8	22	0.26	1.3
182	0.43	50	574	0.13	0.024
2352	5.0	50	161	0.037	0.024

R from R_{GISMF} to R_{max} (fixed Δ), and then increase Δ from Δ_{GISMF} to Δ_{max} (fixed R). Starting from the same baseline GIMMF, another design option is to increase only Δ from Δ_{GISMF} to Δ_{max} , and then increase only R from R_{GISMF} up to R_{max} . A final approach, which serves to derive a bound on $\gamma\kappa$ for large mode area fibers (LMAs), consists in starting from a baseline fiber with $R = R_{\text{max}}$ and $\Delta = \Delta_{\text{min,GI}}$, and then increasing Δ up to Δ_{max} .

We chose $R_{\text{GISMF}} = 6.6 \mu\text{m}$ and $\Delta_{\text{GISMF}} = 0.41\%$, so that $\mathcal{A}_{11} \approx 86 \mu\text{m}^2$, similarly to a standard SMF [45]. We set $\Delta_{\text{max}} = 5\%$, $R_{\text{max}} = 50 \mu\text{m}$, and $\Delta_{\text{min,GI}} = 0.0072\%$. Extreme Δ and R values are considered for maximum generalization. A higher Δ_{max} would tend to break the weak-guidance approximation, and would not be practical since modal delays and MDLs would be too high [13]. The value of R_{max} is bound by fixing a $125 \mu\text{m}$ diameter cladding as for SMFs for device backward compatibility [46], and mechanical reliability [10], [46], [13].

The results of the approach in terms of $\gamma\kappa$ have been plotted in Fig.1, which presents the bounds and the set of achievable values for $\gamma\kappa$. For convenience these have been summarised in Table I for relevant fibers, with their design parameters.

In the following section we analyse in more detail individual parts of the aforementioned approach, to derive approximate closed-form expressions for γ , κ , and $\gamma\kappa$.

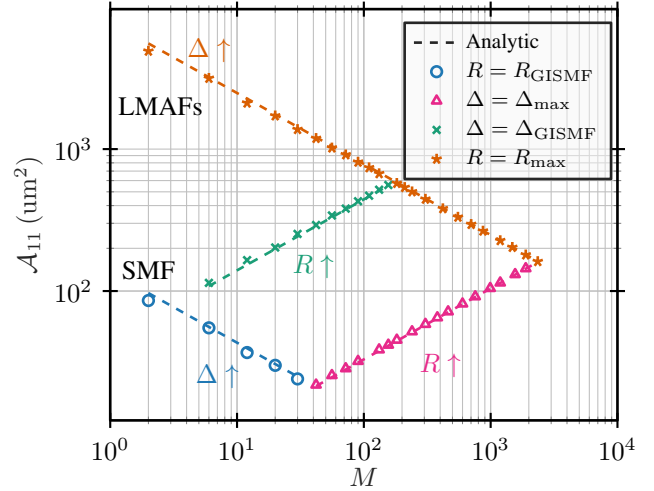


Figure 2: Scaling of \mathcal{A}_{11} with M for different GIMMF designs. Markers indicate numerical results. The dashed lines are the proposed theoretical trends: the line relative to the circles is Eq. (15) with $R = R_{\text{GISMF}}$; the line relative to the triangles is Eq. (12) with $\Delta = \Delta_{\text{max}}$; the line relative to crosses is Eq. (12) with $\Delta = \Delta_{\text{GISMF}}$; the line relative to stars is Eq. (15) with $R = R_{\text{max}}$.

1) *Scaling with the Core Radius:* To study the dependence of $\gamma\kappa$ on R , we consider the set of GIMMFs with increasing M , obtained by increasing R from R_{GISMF} to R_{max} , while keeping Δ fixed to either $\Delta = \Delta_{\text{GISMF}}$ or $\Delta = \Delta_{\text{max}}$. We recently proposed the following approximate closed-form expressions for the fundamental mode effective area and the Manakov nonlinearity coefficient¹ [20]

$$\mathcal{A}_{11} \approx \pi \frac{1}{(\text{NA}k_0)^2} 4\sqrt{M} \quad (12)$$

$$\kappa \approx \frac{M}{M+1} \frac{7}{4\sqrt{M}} \quad (13)$$

Equation 12 has been derived through the Gaussian approximation for the fundamental mode, as detailed in Appendix A. The comparison between the numerical result for \mathcal{A}_{11} and the approximate formula Eq. (12) is visible in Fig. 2 for the cases $\Delta = \Delta_{\text{max}}$ and $\Delta = \Delta_{\text{GISMF}}$.

Equation 13 was obtained in [20] by fitting the numerical results, while in Appendix C we derive analytic results for κ , through the infinite parabolic profile approximation. In particular, the analytic derivation yields the values of κ reported in Table II for any GIMMF up to 32 mode groups (1056 modes). The values turn out to be rational numbers, which are independent on R or Δ alone, but depend solely on M , consistently with the numerical results. The agreement among the analytic, the fitted and the numerical results is visible in Fig. 3, for the cases $\Delta = \Delta_{\text{max}}$ and $\Delta = \Delta_{\text{GISMF}}$.

Equations 12 and 13, with the help of Eq. (2), lead to

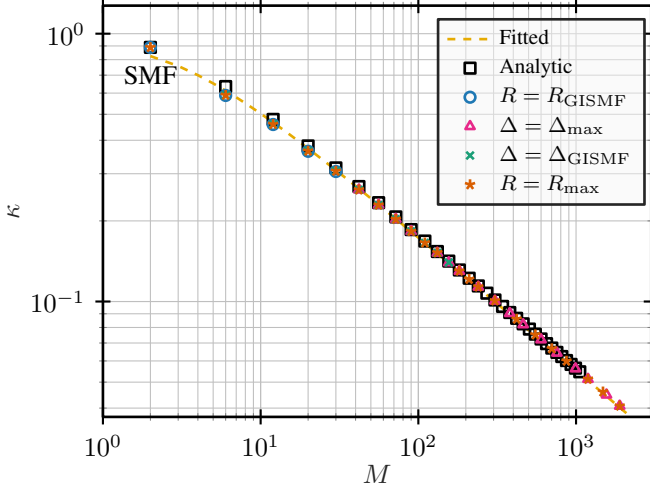
$$\gamma\kappa \approx \frac{\omega_0 n_2}{c} \frac{M}{M+1} \frac{7}{4} \frac{(\text{NA}k_0)^2}{4\pi M} \quad (14)$$

whose agreement with the numerical results is visible in Fig.1, for the cases $\Delta = \Delta_{\text{max}}$ and $\Delta = \Delta_{\text{GISMF}}$.

¹Compared to [20], a factor $\frac{M}{M+1}$ has been prepended to the expression for κ to improve accuracy for small M .

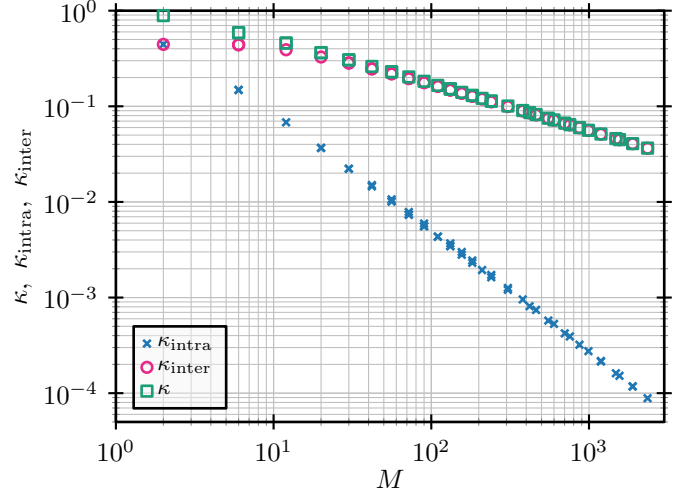
Table II: Analytic values of κ for strongly-coupled GIMMFs with increasing number of guided modes.

M	2	6	12	20	30	42	56	72
κ	8/9	40/63	56/117	8/21	88/279	104/387	40/171	136/657
M	90	110	132	156	182	210	240	272
κ	152/819	56/333	184/1197	200/1413	8/61	232/1899	248/2169	88/819
M	306	342	380	420	462	506	552	600
κ	280/2763	296/3087	104/1143	328/3789	344/4167	40/507	376/4977	392/5409
M	650	702	756	812	870	930	992	1056
κ	136/1953	424/6327	440/6813	152/2439	472/7839	488/8379	56/993	520/9513

**Figure 3:** Scaling of κ with M for different GIMMF designs. Black squares indicate analytic results (from Table II). The other markers represent numerical results. The dashed line is the proposed fitted formula, Eq. (13).

Observe that due to the approximations involved in obtaining Eq. (14), the accuracy for $M = 2$, i.e., the SMF case, is quite bad. A better approximation in this case is Eq. (16).

The intuition behind the trend $\gamma\kappa \propto 1/M$ is that two effects act in the same direction. Firstly, the fundamental mode effective area \mathcal{A}_{11} , which is a measure of how much a mode spreads over a cross-section of the fiber, increases with R , as exemplified by the modal profiles for three different fibers in Fig. 5. Thus, γ reduces as $1/\mathcal{A}_{11}$. Secondly, by its definition Eq. (3), κ is an average of the dimensionless terms $\mathcal{A}_{11}/\mathcal{A}_{ab}$, that are the inverses of the mode effective areas \mathcal{A}_{aa} and of the intermodal effective areas \mathcal{A}_{ab} (when $b \neq a$), normalized by the effective area of the fundamental mode. Note that \mathcal{A}_{ab} is a measure of the overlap between two modes: the larger \mathcal{A}_{ab} , the smaller the overlap. By definition (4), the intermodal area \mathcal{A}_{ab} is no smaller than $\max\{\mathcal{A}_{aa}, \mathcal{A}_{bb}\}$. We can rewrite κ as $\kappa = \kappa_{\text{intra}} + \kappa_{\text{inter}}$, where the term $\kappa_{\text{intra}} \propto 1/N^2 \sum_a \mathcal{A}_{11}/\mathcal{A}_{aa}$ accounts for a (rescaled) average of the inverses of the mode effective areas, and $\kappa_{\text{inter}} \propto 1/N^2 \sum_a \sum_{b \neq a} \mathcal{A}_{11}/\mathcal{A}_{ab}$ for a (rescaled) average of inverses of the intermodal areas. Increasing the number of modes brings into play modes with larger \mathcal{A}_{aa} and \mathcal{A}_{ab} , since the higher order modes are less confined in the core than modes of lower order. Hence, the terms κ_{intra} and

**Figure 4:** Comparison of the contribution of κ_{intra} , accounting for the mode effective areas, and κ_{inter} , accounting for the intermodal effective areas, to $\kappa = \kappa_{\text{intra}} + \kappa_{\text{inter}}$. The values have been computed with the numerical approach for the same MMFs as in Fig. 3.

κ_{inter} have to reduce as it can be observed in Fig. 4. Note that the κ_{intra} becomes negligible for $M \gtrsim 42$ because the summation runs over N terms, while the summation in κ_{inter} runs over $N^2 - N$ terms. In other words, the contribution of the intermodal effective areas significantly outweighs the contribution of the mode effective areas, even though the average of the mode effective areas (with the $1/N$ prefactor) is bigger than the average of the intermodal areas (with the $1/(N^2 - N)$ prefactor).²³ Since both κ_{intra} and κ_{inter} reduce with M , so does κ .

2) *Scaling with the Index Difference:* To study the dependence of $\gamma\kappa$ on Δ , we considered the set of GIMMFs with increasing M , obtained by increasing Δ from Δ_{GISMF} (or from $\Delta_{\text{min,GI}}$) to Δ_{max} , fixed R . We recently proposed the following approximate closed-form expressions [20]

$$\begin{aligned} \mathcal{A}_{11} &\approx \frac{\pi R^2}{\sqrt{M}} \\ \kappa &\approx \frac{M}{M+1} \frac{7}{4\sqrt{M}} \end{aligned} \quad (15)$$

²³This is in contrast to coupled-core MCFs for which the term relative to the intermodal areas vanishes [19].

³Through fitting, we have observed that the average inverse mode effective area (with the $1/N$ prefactor) scales as $\sim 1/M^{0.3}$, and the average inverse intermodal area (with the $1/(N^2 - N)$ prefactor) as $\sim 1/\sqrt{M}$.

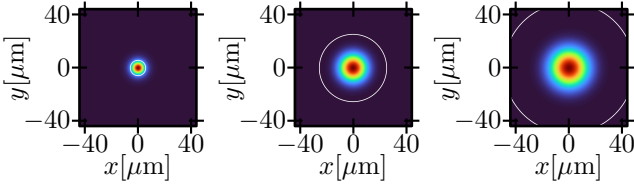


Figure 5: Intensity profiles of the fundamental modes of a set of fibers with increasing R , fixed Δ , and, hence, increasing \mathcal{A}_{11} . The white line indicates the core boundary.

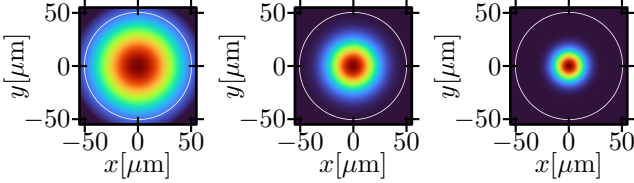


Figure 6: Intensity profiles of the fundamental modes of a set of fibers with increasing Δ , fixed R , and, hence, decreasing \mathcal{A}_{11} . The white line indicates the core boundary.

The derivation of Eq. (15) follows a similar approach to Eq. (12) and is given in Appendix B. The expression for κ is the same as in Section IV-A1, since, as proved in Appendix C, κ depends on M and not on R or on Δ alone. Hence, the analytic values for κ are again the ones in Table II, displayed in Fig. 3.

The comparison between the numerical results and the approximate formulas is visible in Fig. 2 for \mathcal{A}_{11} and in Fig. 3 for κ , for the cases $R = R_{\text{GISMF}}$ and $R = R_{\text{max}}$.

Equations 13 and 15, with the help of Eq. (2), lead to

$$\gamma\kappa \approx \frac{\omega_0 n_2}{c} \frac{M}{M+1} \frac{7}{4} \frac{1}{\pi R^2} \quad (16)$$

where we stress that all the parameters (including R) are constant in this scenario (assuming $M/(M+1) \approx 1$). The comparison between the numerical results and Eq. (16) is given in Fig.1 for the cases $R = R_{\text{GISMF}}$ and $R = R_{\text{max}}$, where it can be seen that $\gamma\kappa$ remains nearly constant as Δ is scaled.

The intuition behind the (quasi-)constant behavior of $\gamma\kappa$ in this scenario is that two effects balance each other out. The first is that \mathcal{A}_{11} reduces with Δ , since the fundamental mode gets more confined in the core, as exemplified by the modal profiles for three different fibers in Fig.6. Thus, $\gamma \propto 1/\mathcal{A}_{11}$ increases. On the other hand, κ decreases with M for the same qualitative reason as in the previous section. Indeed, given that κ does not depend on the absolute values of the mode effective areas and of the intermodal effective areas, but on their value normalized by the fundamental mode effective area, the reduction of \mathcal{A}_{11} and \mathcal{A}_{ab} does not affect the reduction of the dimensionless $\mathcal{A}_{11}/\mathcal{A}_{ab}$ terms. In other words, increasing the number of modes brings still into play modes with smaller $\mathcal{A}_{11}/\mathcal{A}_{ab}$ terms. Given that these terms enter the averaging definition of κ , κ reduces with M in the same manner as in Section IV-A1.

It is worth mentioning that Eq. (14) and Eq. (16) are in fact valid for any GIMMF, even when Δ and R are varied together. The disadvantage of using the two formulas for a different case than the one they have been developed for is that the link

between $\gamma\kappa$ and M becomes hidden behind NA for Eq. (14) and behind R for Eq. (16). Despite that, Eq. (16) is a better approximation than Eq. (14) for small M , also for the cases for which Eq. (14) has been developed.

Finally, observe from Fig.1 that the scaling of $\gamma\kappa$ with M is not simply $1/M$, but depends on the strategy to increase M – subject to the consideration of the linear effects (e.g., modal dispersion) [33], [13]. The $\gamma\kappa \propto 1/M$ scaling is possible only for $M \gtrsim 200$. A design strategy with poor $\gamma\kappa$ roll-off with M , as for fixed R , may lead to enhanced nonlinearities, as discussed in Section VI.

B. Weak Coupling Regime

In the case of the WCR, the nonlinear coupling coefficients form a symmetric square matrix $\gamma\kappa$ – whose size matches the number of mode groups. To find a closed-form expression for that, we can approximate again γ and κ separately. The γ coefficient can be expressed through Eq. (12) or Eq. (15) as before. In Appendix C we derived the analytic κ_{ab} reported in Table III for a GIMMF up to the first 10 groups (110 polarization modes), regardless of whether R and/or Δ are varied. The analytic κ_{ab} for a GIMMF up to the first 32 groups (1056 polarization modes) are provided in [47]. In addition, we propose the following simple relation obtained by fitting the numerical results

$$\kappa_{ab} \approx \frac{4}{3} \frac{M_a}{M_a + \delta_{ab}} \frac{1}{\max\{a, b\}} \quad (17)$$

where $M_a = 2a$ is the number of modes in group a . It can be observed that the fitted formula (17) yields the exact same values as the analytic results of Table III.

Fig. 7 compares the analytic/fitted values of κ with the numeric ones. The error between them has been computed as

$$\frac{1}{G^2} \sum_{a=1}^G \sum_{b=1}^G \frac{|\kappa_{ab} - \tilde{\kappa}_{ab}|}{\kappa_{ab}} \quad (18)$$

where with $\tilde{\kappa}_{ab}$ we indicated the values obtained with the analytic expression Eq. (17) to distinguish them from the ones obtained numerically, which we indicated as κ_{ab} . A plot for the error metric (18) is reported in Fig. 8. The analytic result is exact for an SMF, the error is $\sim 7\%$ for a 6-modes (or 2 groups) GIMMFs, and reduces to below 0.6% for a 992-modes (or 31 groups) GIMMFs.

Finally, observe that within our approximations the κ matrices do not depend on the number of fiber modes, such that for any two GIMMFs with M_1 and M_2 modes respectively, and $M_2 > M_1$, κ for the M_1 -modes fiber is a submatrix of the κ for the M_2 -modes fiber. Hence, the data in Table III are valid for the κ_{ab} of the first 10 mode groups of any GIMMF, and the ones in [47] for the first 32 mode groups.

C. Step-Index Fibers

Even though employing SIMMFs for long-haul communications might be even more challenging than utilizing GIMMFs due to a larger delay spread [10], scaling trends are derived here for the sake of completeness.

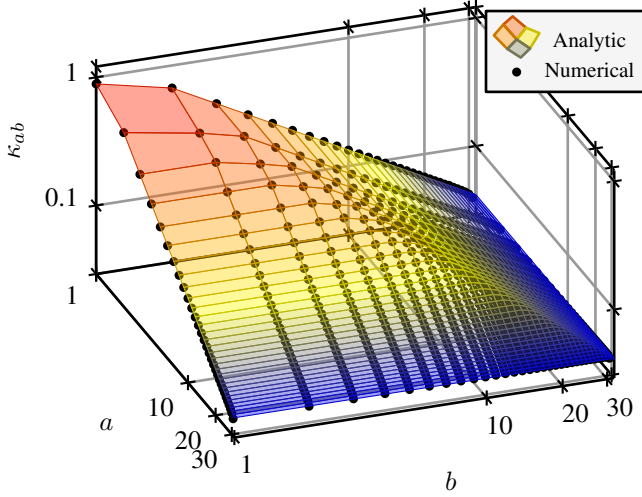


Figure 7: Comparison between the analytic κ (represented as a surface) and the numerical κ for a GIMMF with 31 mode groups.

Table III: Analytic values of κ_{ab} for a GIMMF up to 10 mode groups. The analytic κ_{ab} for a GIMMF up to the first 32 groups (1056 modes) are provided in [47].

$a \setminus b$	1	2	3	4	5	6	7	8	9	10
1	$\frac{8}{9}$	$\frac{2}{3}$	$\frac{4}{9}$	$\frac{1}{3}$	$\frac{4}{15}$	$\frac{2}{9}$	$\frac{4}{21}$	$\frac{1}{6}$	$\frac{4}{27}$	$\frac{2}{15}$
2	$\frac{2}{3}$	$\frac{8}{15}$	$\frac{4}{9}$	$\frac{1}{3}$	$\frac{4}{15}$	$\frac{2}{9}$	$\frac{4}{21}$	$\frac{1}{6}$	$\frac{4}{27}$	$\frac{2}{15}$
3	$\frac{4}{9}$	$\frac{4}{9}$	$\frac{8}{21}$	$\frac{1}{3}$	$\frac{4}{15}$	$\frac{2}{9}$	$\frac{4}{21}$	$\frac{1}{6}$	$\frac{4}{27}$	$\frac{2}{15}$
4	$\frac{1}{3}$	$\frac{1}{3}$	$\frac{1}{3}$	$\frac{8}{27}$	$\frac{4}{15}$	$\frac{2}{9}$	$\frac{4}{21}$	$\frac{1}{6}$	$\frac{4}{27}$	$\frac{2}{15}$
5	$\frac{4}{15}$	$\frac{4}{15}$	$\frac{4}{15}$	$\frac{4}{15}$	$\frac{8}{33}$	$\frac{2}{9}$	$\frac{4}{21}$	$\frac{1}{6}$	$\frac{4}{27}$	$\frac{2}{15}$
6	$\frac{2}{9}$	$\frac{2}{9}$	$\frac{2}{9}$	$\frac{2}{9}$	$\frac{2}{9}$	$\frac{8}{39}$	$\frac{4}{21}$	$\frac{1}{6}$	$\frac{4}{27}$	$\frac{2}{15}$
7	$\frac{4}{21}$	$\frac{4}{21}$	$\frac{4}{21}$	$\frac{4}{21}$	$\frac{4}{21}$	$\frac{4}{21}$	$\frac{8}{45}$	$\frac{1}{6}$	$\frac{4}{27}$	$\frac{2}{15}$
8	$\frac{1}{6}$	$\frac{8}{51}$	$\frac{4}{27}$	$\frac{2}{15}$						
9	$\frac{4}{27}$	$\frac{8}{57}$	$\frac{2}{15}$							
10	$\frac{2}{15}$	$\frac{8}{63}$								

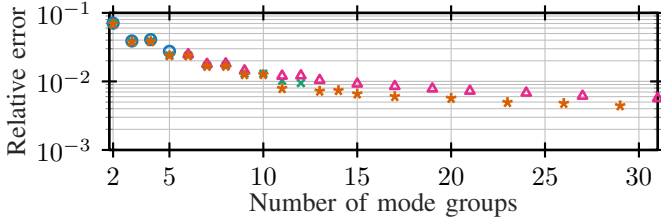


Figure 8: Average relative error (18) between the analytic and the numeric κ for each GIMMF of Fig. 1 up to 31 groups. The SMF case is not displayed as the error is 0. Markers as in Fig. 1.

The same approach as the one devised to study GIMMFs is employed here for SIMMFs. The chosen starting point is a fiber with $R_{\text{SISMF}} = 4.1 \mu\text{m}$ and $\Delta_{\text{SISMF}} = 0.32\%$, to mimic a SSMF with $\mathcal{A}_{11} = 85 \mu\text{m}^2$ [45]. The other relevant parameters are $R_{\text{max}} = 50 \mu\text{m}$, $\Delta_{\text{min,SI}} = 0.0034\%$, and $\Delta_{\text{max}} = 5\%$. Based on the numerical results, we found the same trends as

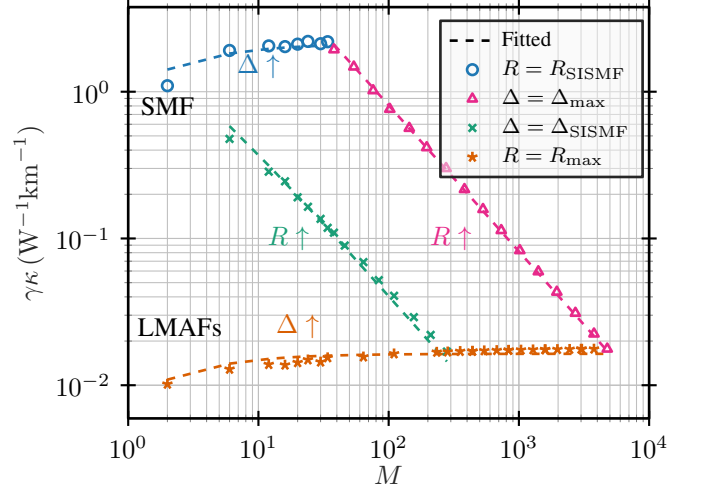


Figure 9: Scaling of $\gamma\kappa$ with M for different SIMMF designs. Markers indicate numerical results. The dashed lines are the trends in Eq. (19) with fitted proportionality factors.

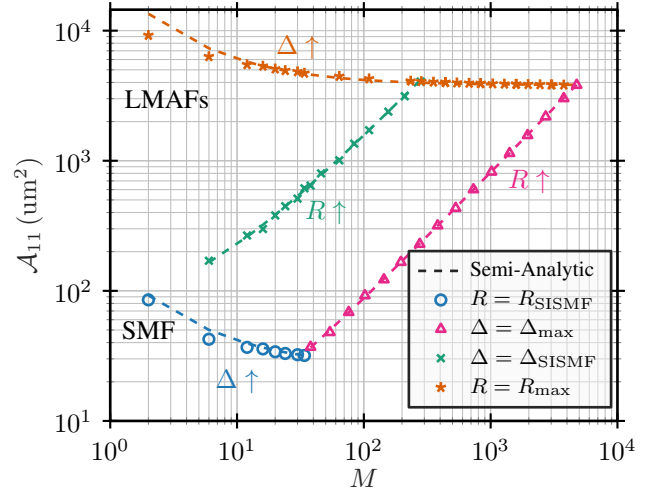


Figure 10: Scaling of \mathcal{A}_{11} with M for different SIMMF designs. Markers indicate numerical results. The dashed lines are theoretical trends (but with fitted proportionality factors!): the line relative to the circles is Eq. (59) with $R = R_{\text{SISMF}}$; the line relative to the triangles is Eq. (58) with $\Delta = \Delta_{\text{max}}$; the line relative to the crosses is Eq. (58) with $\Delta = \Delta_{\text{SISMF}}$; the line relative to the stars is Eq. (59) with $R = R_{\text{max}}$.

GIMMFs to approximately hold, that is,

$$\gamma\kappa \propto \begin{cases} 1/(M+1), & \text{if } R \text{ is varied fixed } \Delta \\ M/(M+1), & \text{if } \Delta \text{ is varied fixed } R \end{cases} \quad (19)$$

where the proportionality factors can be obtained by fitting the numerical results, as displayed in Fig. 9. The scaling of \mathcal{A}_{11} and κ with number of modes when varying R and Δ are displayed in Fig. 10 and in Fig. 11, including the semi-analytic approximation of \mathcal{A}_{11} reported in Appendix E. Given the lower interest in SIMMFs for long-haul communications compared to GIMMFs, we do not provide an analytic result for κ , even though a more quantitative discussion is carried out in Appendix E.

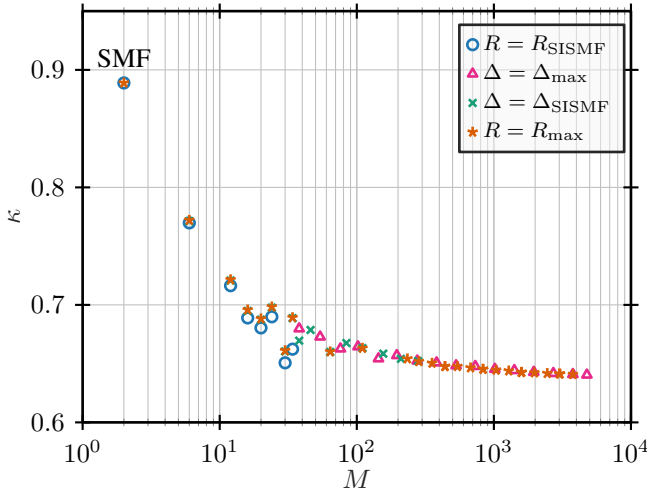


Figure 11: Scaling of κ with M for different SIMMF designs.

V. OPTIMIZED AND MANUFACTURED FIBERS

In Fig. 12 the $\gamma\kappa$ values for different optimized and/or manufactured GIMMFs described in the literature have been reported against the developed framework, assuming to operate in the SCR. Such fibers have been emulated based on the available information in the respective references, which did not always include all the necessary data about the refractive index profile. Hence, some little discrepancies between the actual $\gamma\kappa$ and the one computed by us are possible. Nevertheless, the consistency between the $\gamma\kappa$ computed for the fibers in the literature and our framework supports the validity of our investigation. In particular, the optimized fibers lie within the foreseen boundaries, and the approximate trends for $\gamma\kappa$ ($\propto 1/M$ with R , and const with Δ), are verified again. Similar considerations hold for \mathcal{A}_{11} and κ .

It should be noted that the optimized and manufactured fibers in general exploit more advanced index profiles, which would formally require an extension to the analysis in this paper for a proper comparison. At the same time, we verified that the κ computed (through the numerical method) for the literature fibers, which exploit trenches and grading indices slightly different from 2, are close to the κ of the trenchless parabolic GIMMFs. In addition, a quantitative reasoning based on the Gaussian approximation for the effective area of a generic GI profile suggests that for realistic slightly non-parabolic GIs $\gamma\kappa$ deviates by at most 10% from the parabolic case, see Appendix F.

The fiber data used for the plots of the paper, including the fibers emulated from the literature, and additional data like the intermodal effective areas \mathcal{A}_{ab} have been provided in [47].

VI. CONSIDERATIONS ON DATA RATES

The ultimate throughput limit of an SDM system in the SCR depends on Kerr nonlinearity, which depends also on $\gamma\kappa$. In order to study the impact of the scaling of $\gamma\kappa$ with M on the data rates of GIMMF systems, let us consider the perturbative model developed in [23]. The model assumes a strongly-coupled SDM fiber with only strong linear coupling, mode-independent chromatic-dispersion (CD) and Kerr nonlinearity

as distortions. No other linear effects like modal delay or MDL are included. Ideal distributed amplification able to perfectly compensate the fiber loss is assumed. Circularly-symmetric complex Gaussian modulation is considered. Compensation of the linear effects (coupling and CD) is assumed through, e.g., DSP. Digital back-propagation (DBP) is potentially applied on the channel under test, so that self-phase modulation (SPM) is removed. The mean phase noise is also removed. In such case, the achievable information rate in terms of bit/s/Hz/mode for an additive white Gaussian noise (AWGN) receiver can be computed as

$$R(M, P) = \log_2 \left(1 + \frac{P}{N_{\text{ASE}}B + \sigma_{\text{NLI}}^2} \right) \quad (20)$$

where P is the transmit power per channel per mode, N_{ASE} is the amplified spontaneous emission (ASE) noise flat power spectral density (PSD) over a band $B = 1/T$, T is the symbol time, and σ_{NLI}^2 is the variance of the equivalent nonlinear interference noise. It holds $\sigma_{\text{NLI}}^2 = (\gamma\kappa)^2 (\eta_2 M^2 + \eta_1 M + \eta_0) P^3$, where η_x for $x \in \{0, 1, 2\}$ are coefficients whose computation is described in [23]. For the examples below we considered a root-raised cosine shaping pulse with roll-off factor 0.1 and no DBP.

Neglecting η_2 (realistic for $M \leq 1000$) and η_0 (rendered negligible for $M > 10$ since $\eta_0 = \eta_1$ in our setup [23]), and fixing the power per mode P , it follows that the scaling of the nonlinear interference σ_{NLI}^2 , and thus of the data rate per mode, depends on $(\gamma\kappa)^2 (\eta_1 M)$. In particular, if $\gamma\kappa$ reduces with number of modes faster than $1/\sqrt{M}$, the data rate increases with the number of modes. This would imply that a MMF could achieve a higher data rate than a bundle of SMFs with same total number of modes, fixed the same power per mode. This is depicted in Fig. 13 for a) the best-case scenario $\gamma\kappa \propto 1/M$ and for b) the (approximate) limiting one $\gamma\kappa \propto 1/\sqrt{M}$; η_0 and η_2 were not neglected in Fig. 13, and the parameter setup of [23, Table I-II] was used. The different data rate scaling trends in Fig. 13a and Fig. 13b highlight the importance of designing a fiber keeping into account nonlinearity and, hence, $\gamma\kappa$. Previously [19], [55], the data rate of MMFs was believed to increase with M , while as we showed this is valid only when $\gamma\kappa \propto 1/M$, which is correct only for a specific way of designing fibers, that is, by only increasing R . Note that similar conclusions could be reached with other perturbative models in the literature like the ones in [19], [56], [21].

Observe that (20) can be exploited to assess once more the accuracy of the derived analytic and fitted expressions for $\gamma\kappa$ in the SCR. We verified that using Eq. (2) for computing γ and the analytic values of Table II for computing κ , instead of the numerical $\gamma\kappa$, would introduce an error in the rate computation below 0.8% for a 6-modes MMF and below 0.02% for a 992-modes MMF. Using Eq. (2) for computing γ and the fitted values (16) for κ , instead of the numeric $\gamma\kappa$, would introduce an error below 2.3% for a 6-modes MMF and below $\sim 0.2\%$ for a 992-modes MMF. The error metric we adopted is $|R - \hat{R}|/R$, where in this case by R we mean the rate computed via the numeric $\gamma\kappa$, while by \hat{R} we mean the rate computed via either the analytic or the fitted $\gamma\kappa$. The low error confirms the validity

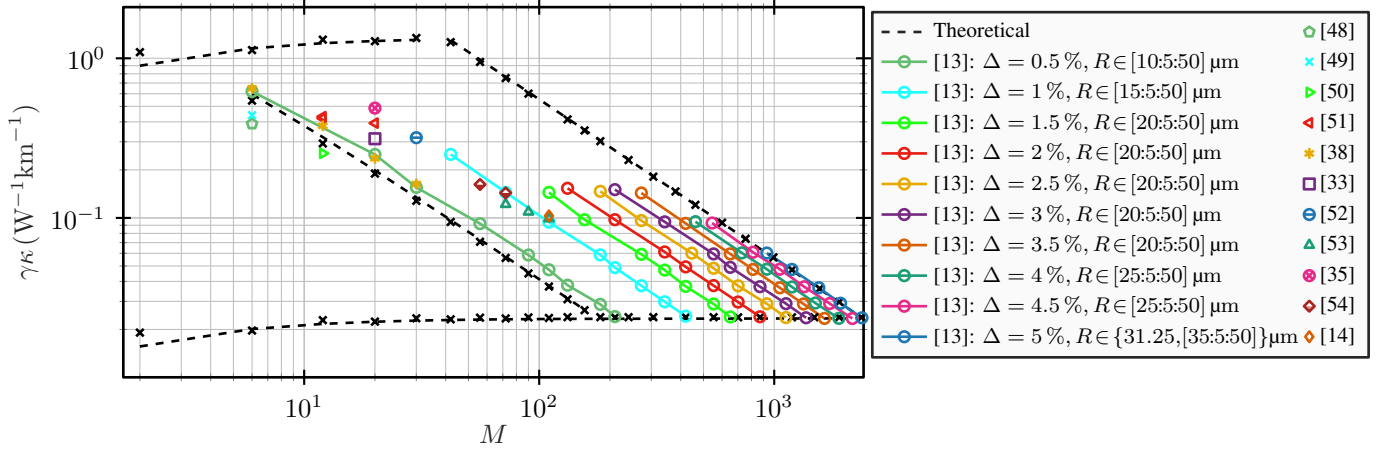


Figure 12: Scaling of γ_{κ} with M for a number of optimized and manufactured GIMMFs. The notation $R \in [a:b:c]$ in the legend indicates that, moving from top to bottom along a line, the first point refers to a fiber with $R = a$, the second point refers to a fiber with $R = a + b$, and so on until the last fiber with $R = c$. Dashed lines and crosses refer to the same lines and points as in Fig. 1.

of the analytic and fitted formulas for the described scenario, in particular for MMFs with a not too small M .

It is worth mentioning that SDM systems are being investigated in the literature for very different transmission scenarios which might not correspond to the one presented in this section. In particular, the data rate per mode with fixed the power per mode might not be the relevant metric in all situations. Thus, the example discussed above is meant as an application of the γ_{κ} study rather than a general statement on the usefulness of SDM systems.

Finally, data rates have been computed in this Section considering only chromatic-dispersion and Kerr nonlinear effect, since the purpose is to highlight the role of γ_{κ} and of fiber design in such scenarios, rather than proposing accurate estimates of data rates for SDM systems. However, more relevant effects which reduce data rates and which we neglected are the presence of potential uncompensated inter-group linear coupling in the WCR [57], and in general any residual presence of linear coupling [58], which should be accounted for in a thorough rate analysis of SDM systems. Other impairments, which have been neglected, but which are expected to play a non-negligible role in terms of rate reduction are MDL, bend losses, and coating losses [13]. The interplay between the mention linear effects (with the inclusion of mode delay) and Kerr nonlinear effects should also be considered, as already partially done in, e.g., [59], [19], [21], [22]. Even though complete compensation of the linear effects has been assumed for Eq. (20), the computational burden of the DSP algorithms for increasing number of modes has not been addressed, which is a well-known open challenge [10], [1].

VII. SIDE REMARKS

Some aspects related to assumptions made throughout the papers are worth to be discussed.

Firstly, we assumed the hypotheses of Manakov equations for the SCR and the WCR to be fulfilled, i.e., the right levels of cross-talk (XT) (a metric for the intensity of linear coupling [29]) among the various mode groups, and a not too large

difference between the maximum and the minimum mode delays for strongly coupled modes [19], [30]. The level of XT between two modes depends on both the phase-mismatch between them and the fiber perturbations inducing linear coupling [60], [7], [61], [29]. Hence, given a certain fiber, there is no a-priori regime of linear coupling in which it operates; the regime depends on the level of XT, which depends on the environment and on the system architecture. In practical scenarios the two regimes which we considered might be hard to achieve, with the intermediate coupling regime being often the actual one [29], [30], [31]. At the same time, techniques have been proposed to intentionally increase the level of XT to achieve the SCR when desired, as mentioned in Section I. Concerning the WCR, it is in practice hard to ensure no inter-group coupling at all as it is hard to almost completely remove the impact of the perturbations. However, fiber designs with high Δ tend to be more favorable in this sense [1].

Another relevant point to discuss is the assumption of weak-guidance. Since the weak-guidance approximation for which LP modes exist is typically assumed in the literature for fibers with $\Delta < 1\%$ [40, p.38] [44, p.20], it might have been the case that such approximation did not hold for the MMFs considered in this paper for which $\Delta \in [1\%, 5\%]$. Thus, the accuracy of the numerical results has been checked for some points of Fig.1, including some for which $\Delta = 5\%$, generating the vector-modal profiles with the mode solver implemented in MATLAB as described in [39] and based on [62].⁴ A square grid of $N_p \times N_p$ evenly spaced points (with $N_p \geq 600$) has been used, covering a square integration area with edge length of $125 \mu\text{m}$. For the fibers we tested, we observed a maximum discrepancy between the elements of κ computed with the LP and with the vector mode solver below 2% (and much lower in terms of κ in the SCR), justifying the adoption of the LP solver (mentioned in Section III), which is computationally less expensive. The number of guided modes for each generated

⁴The mode solver described in [62] is freely accessible as “Thomas Murphy (2024). Waveguide Mode Solver (<https://www.mathworks.com/matlabcentral/fileexchange/12734-waveguide-mode-solver>), MATLAB Central File Exchange. Retrieved August 12, 2024.”

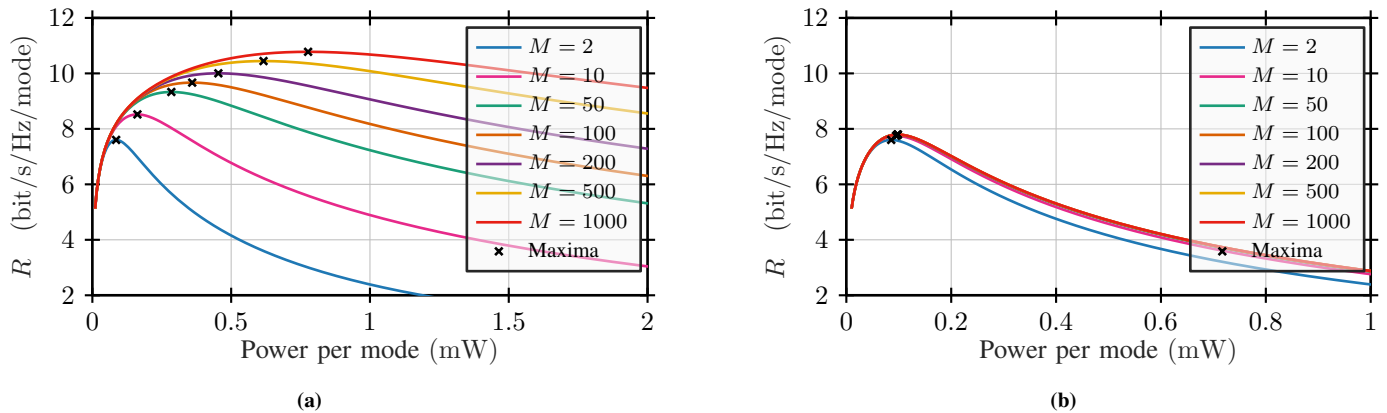


Figure 13: Comparison between the achievable data rates computed with Eq. (20) when $\gamma\kappa \propto 1/M$ (13a), and when $\gamma\kappa \propto 1/\sqrt{M}$ (13b), within the perturbation model and the assumptions of [23].

fiber in the weak-guidance has also been compared against the number of guided vector modes without such assumption [63], finding negligible discrepancies.

VIII. CONCLUSIONS

We have investigated the scaling of the nonlinear coupling coefficients $\gamma\kappa$ and $\gamma\kappa$, appearing in the Manakov equations for the SCR and the WCR, respectively, with the number of modes M .

Closed-form expressions have been derived, which depend on few fiber design parameters, namely, core radius R , refractive index difference between core and cladding Δ , and number of guided modes. Validation has been performed with a numerical approach. The closed-form expressions provide a significantly quicker tool to compute $\gamma\kappa$ and $\gamma\kappa$. Our analysis indicates that the elements of κ are simple rational numbers which depend only on M . As γ depends on the fundamental mode effective area \mathcal{A}_{11} , which increases with R and reduces with Δ , maximizing \mathcal{A}_{11} minimizes the elements of $\gamma\kappa$, for a fixed M .

Even though the analysis has been carried out for trenchless parabolic GIMMFs, the comparison with values of $\gamma\kappa$ computed for optimized and manufactured MMFs confirms the validity of our approach for realistic fiber designs employing trenches and non-parabolic graded-index profiles.

The insights developed in this paper can be helpful for fiber design, and the closed-form expressions can be used, e.g., in nonlinear SDM channel models [21], [22], [23]. Thus, contributing towards the assessment of the feasibility of a future long-haul SDM communication system.

APPENDIX A

CLOSED-FORM EXPRESSION FOR THE FUNDAMENTAL EFFECTIVE AREA OF GIMMFs: VARYING THE CORE RADIUS

In order to obtain an approximate analytic expression for \mathcal{A}_{11} when varying only R , let the fundamental mode be approximated with a Gaussian function as [44, Eq. 15-2] [28, Eq. 2.2.38] [32, Eq. 2.74]

$$c \exp\left(\frac{\rho}{r_0}\right)^2 \quad (21)$$

where $c \geq 0$ is some scaling factor, ρ is the radial coordinate, r_0 is the so-called spot-size. Then, the fundamental mode effective area becomes [28, p. 32]

$$\mathcal{A}_{11} = \pi r_0^2 \quad (22)$$

The spot-size r_0 can be related to V through different approaches. An empirically-fitted formula is [64, Eq. 11]

$$\frac{r_0}{R} = \frac{A}{\sqrt{V}} + \frac{B}{V^{1.5}} + \frac{C}{V^6} \quad (23)$$

with $A = \sqrt{2}$, $B \approx 0.372$, and $C \approx 26.773$. For the case of a parabolic GIMMF, the last two terms are relevant only for low values of V (and thus M). Hence, we neglect them for the sake of simplicity. A similar relation can be obtained with a variational approach, through which it has been shown that, for the infinite parabolic refractive index profile, [44, Table 14-2]

$$\frac{r_0}{R} \propto \frac{1}{\sqrt{V}} \quad (24)$$

where \propto means ‘‘proportional to’’. A similar dependence has been obtained for the Gaussian refractive index profile [44, Table 15-2].

From Eq. (22) and Eq. (23), it turns out that

$$\mathcal{A}_{11} \approx \pi \frac{2R^2}{V} \quad (25)$$

Expressing R in terms of V , substituting Eq. (10) in Eq. (25), and remembering that Δ is fixed (i.e., M changes only because of R), yields

$$\mathcal{A}_{11} \approx \pi \left(\frac{1}{NAk_0} \right)^2 4\sqrt{M}$$

APPENDIX B

CLOSED-FORM EXPRESSION FOR THE FUNDAMENTAL EFFECTIVE AREA OF GIMMFs: VARYING THE REFRACTIVE INDEX DIFFERENCE

The approximate closed formula for \mathcal{A}_{11} when R is fixed can be retrieved with the same Gaussian approach employed in Appendix A. With the help of Eq. (25) and Eq. (10),

remembering that this time R is fixed and Δ varies, it is found that

$$A_{11} \approx \frac{\pi R^2 A^2}{2} \frac{1}{\sqrt{M}}$$

APPENDIX C

ANALYTIC EXPRESSION FOR THE MANAKOV NONLINEARITY COEFFICIENTS OF GIMMFs

In this section we derive approximate analytic results for the generic nonlinearity coefficient $\kappa_{\alpha\beta}$ of the matrix κ for GIMMFs defined by Eq. (3). We remind that κ reduces to the scalar κ in case of a single group of strongly-coupled modes.

In order to derive an approximate analytic expression for $\kappa_{\alpha\beta}$ for GIMMFs, the infinite parabolic profile approximation can be exploited, which provides relatively simple analytic expressions for the modal profiles, while for the actual parabolic profile of Eq. (8) the analytic expression would be more complicated, involving the Whittaker functions of the first kind [44, Sec. 14-8]. This approach is commonly employed to obtain closed-form expressions for relevant quantities of GIMMFs like propagation constants and their relative cutoff values [28, Sec.11.2.2], modal profiles, and nonlinear coefficients [65]. The approximation consists in assuming that the refractive index profile is parabolic everywhere, not only in the core. That is, it assumes that Eq. (8) holds also for $\rho > R$. The approximation is reasonable for low-order modes and a large enough core radius R [28, Sec.11.2.2], even though we successfully exploit it for all modes and core radii later.

The modal profiles are then [44, Table 14-2][65]

$$\mathbf{F}_{p,m}(\rho, \varphi) = \tilde{F}_{p,m}(\rho) \mathbf{p}_m(\varphi) \quad (26)$$

where p and m are two integers, ρ is the radial coordinate, φ is the azimuth coordinate, and [65]

$$\tilde{F}_{p,m}(\rho) = A_p^m \frac{\rho^m}{\rho_0^{m+1}} e^{-\frac{\rho^2}{2\rho_0^2}} L_p^m \left(\frac{\rho^2}{\rho_0^2} \right) \quad (27)$$

where L_p^m is a generalized Laguerre polynomial. The quantity $\tilde{F}_{p,m}(\rho)$ accounts for the radial dependence of the modal profile with

$$A_p^m = \sqrt{\frac{p!}{\pi (p+m)!}} \quad (28)$$

$$\rho_0 = \frac{R}{(4N_2)^{1/4}} \quad (29)$$

$$N_2 = \frac{1}{2} n_0^2 k_0^2 R^2 \Delta \quad (30)$$

The coefficient A_p^m has been chosen to fulfill the following orthonormality condition among the modes [65, Eq.5]

$$\int_0^{2\pi} \int_0^\infty \rho \mathbf{F}_{p',m'}^*(\rho, \varphi) \mathbf{F}_{p,m}(\rho, \varphi) d\rho d\varphi = \delta_{p,p'} \delta_{m,m'} \quad (31)$$

The L_p^m are the generalized Laguerre polynomials which can be expressed in different ways. A handy approach for us is [66, Eq. 18.59]

$$L_p^m(\rho) = \sum_{i=0}^n b_i(n, m) \rho^i \quad (32)$$

where

$$b_i(n, m) = (-1)^i \binom{p+m}{p-i} \frac{1}{i!} \quad (33)$$

With simple algebraic passages we derived the following expression which can speed up the numerical implementation

$$b_{i+1}(p, m) = -\frac{p-i}{(i+1)(m+i+1)} b_i(p, m) \quad (34)$$

The expression of the polarization and azimuth dependence $\mathbf{p}_m(\varphi)$ appearing in Eq. (26) depends on the chosen modal basis. Note that, in case of the LP modes, to draw a link with the classic notation, the mode $\mathbf{F}_{p,m}$ corresponds to LP $_{m,p+1}$ [44, p. 308]. In case of vector modes, within weak-guidance, the expressions for the polarization vectors $\mathbf{p}_m(\varphi)$ are [67, Eq. 1]

$$\begin{cases} p \geq 0 \\ \text{TM}_{0,p+1}(\varphi) = \cos(\varphi) \hat{\mathbf{x}} + \sin(\varphi) \hat{\mathbf{y}} \\ \text{TE}_{0,p+1}(\varphi) = \sin(\varphi) \hat{\mathbf{x}} - \cos(\varphi) \hat{\mathbf{y}} \end{cases} \quad (35)$$

$$\begin{cases} m > 1, p \geq 0 \\ \text{EH}_{m-1,p+1}^e(\varphi) = \cos(m\varphi) \hat{\mathbf{x}} + \sin(m\varphi) \hat{\mathbf{y}} \\ \text{EH}_{m-1,p+1}^o(\varphi) = \sin(m\varphi) \hat{\mathbf{x}} - \cos(m\varphi) \hat{\mathbf{y}} \end{cases} \quad (36)$$

$$\begin{cases} m \geq 1, p \geq 0 \\ \text{HE}_{m+1,p+1}^e(\varphi) = \cos(m\varphi) \hat{\mathbf{x}} - \sin(m\varphi) \hat{\mathbf{y}} \\ \text{HE}_{m+1,p+1}^o(\varphi) = \sin(m\varphi) \hat{\mathbf{x}} + \cos(m\varphi) \hat{\mathbf{y}} \end{cases} \quad (37)$$

Note that all modal bases obtained as a unitary transformation of (quasi-)degenerate vector modes lead to the same $\gamma_{\kappa_{\alpha\beta}}$ [41], [42]. Hence, in principle the LP and vector modal basis are equivalent. However, we adopt the vector modes since they simplify the calculations later on.

Starting from Eqs. 6, 4, and 7, the generic nonlinearity coefficient $\kappa_{\alpha\beta}$ can be computed as

$$\kappa_{\alpha\beta} = \frac{4}{3} \frac{1}{(2N_\alpha + \delta_{\alpha,\beta}) 2N_\beta} \sum_{a \in I_\alpha} \sum_{b \in I_\beta} A_{11} D_{ab} \quad (38)$$

where we exploited the orthonormality so that $\int_{-\infty}^\infty \int_{-\infty}^\infty \|\mathbf{F}_a\|^2 dx dy = \int_{-\infty}^\infty \int_{-\infty}^\infty \|\mathbf{F}_b\|^2 dx dy = 1$, and we defined

$$D_{ab} = \int_0^\infty \int_0^{2\pi} \rho \|\mathbf{F}_a\|^2 \|\mathbf{F}_b\|^2 d\varphi d\rho \quad (39)$$

where a stands for the pair of mode indices (p, m) and b stands for (s, v) . Hence, we now derive a closed-form expression for D_{ab} .

Note that Eq. (6) has been originally derived for LP modes only, while for vector modes a (slightly) more complex expression is normally used [19, Eq. 56]. We show in Appendix D that Eq. (6) holds also for vector modes (within weak-

guidance) and hence we are allowed to consider Eq. (39) for vector modes as well.⁵ Then,

$$\begin{aligned} D_{ab} &= \int_0^\infty \int_0^{2\pi} \rho \|\tilde{F}_{p,m}(\rho) \mathbf{p}_m(\varphi)\|^2 \|\tilde{F}_{s,v}(\rho) \mathbf{p}_v(\varphi)\|^2 d\varphi d\rho \\ &= 2\pi \int_0^\infty \rho \|\tilde{F}_{p,m}(\rho)\|^2 \|\tilde{F}_{s,v}(\rho)\|^2 d\rho \end{aligned} \quad (40)$$

where we made use of $\|\mathbf{p}_m(\varphi)\|^2 = \|\mathbf{p}_v(\varphi)\|^2 = 1$, thanks to our choice of modal basis.

Substituting Eq. (27) into Eq. (40)

$$\begin{aligned} D_{ab} &= \tilde{C}_{ab} \int_0^\infty \rho \rho^{2m+2v} e^{-2\frac{\rho^2}{\rho_0^2}} L_p^m \left(\frac{\rho^2}{\rho_0^2} \right) \\ &\quad L_p^m \left(\frac{\rho^2}{\rho_0^2} \right) L_s^v \left(\frac{\rho^2}{\rho_0^2} \right) L_s^v \left(\frac{\rho^2}{\rho_0^2} \right) d\rho \end{aligned} \quad (41)$$

where $\tilde{C}_{pmsv} = 2\pi \left(\frac{A_p^m A_s^v}{\rho_0^{m+1} \rho_0^{v+1}} \right)^2$ and \tilde{C}_{ab} is a short-hand notation for \tilde{C}_{pmsv} . We perform the change of variable $u = \rho^2$, so that $du = 2\rho d\rho$, which yields

$$\begin{aligned} D_{ab} &= C_{ab} \int_0^\infty u^{\tau_{mv}} e^{-\sigma u} L_p^m \left(\frac{u}{\lambda} \right) L_p^m \left(\frac{u}{\lambda} \right) \\ &\quad L_s^v \left(\frac{u}{\lambda} \right) L_s^v \left(\frac{u}{\lambda} \right) du \end{aligned} \quad (42)$$

where $C_{ab} = \tilde{C}_{ab}/2 = \pi \left(\frac{A_p^m A_s^v}{\rho_0^{m+v+2}} \right)^2$, $\tau_{mv} = m+v$, $\sigma = \rho_0^2/2$, and $\lambda = \rho_0^2$. We now follow similar steps to [68] to retrieve a closed-form expression for the previous formula. Plugging Eq. (32) into Eq. (42), it is obtained

$$\begin{aligned} D_{ab} &= C_{ab} \sum_{i=0}^p \sum_{j=0}^p \sum_{k=0}^s \sum_{l=0}^s b_i(p, m) b_j(p, m) \\ &\quad b_k(s, v) b_l(s, v) \lambda^{\varepsilon - \tau_{mv}} \int_0^\infty e^{-\sigma u} u^\varepsilon du \end{aligned} \quad (43)$$

where $\varepsilon = i + j + k + l + \tau_{mv}$. With the change of variable $x = \sigma u$, the integral $\int_0^\infty e^{-\sigma u} u^\varepsilon du$ becomes

$$\sigma^{-(\varepsilon+1)} \int_0^\infty e^{-x} x^\varepsilon dx = \sigma^{-\varepsilon+1} \Gamma(\varepsilon+1) = \sigma^{-(\varepsilon+1)} \varepsilon! \quad (44)$$

where the last passage holds only for integer values of ε , and where $\Gamma(\varepsilon+1) = \int_0^\infty e^{-x} x^\varepsilon dx$ is the well-known gamma function. Observe also that $C_{ab} \lambda^{\varepsilon - \tau_{mv}} \sigma^{-(\varepsilon+1)} = C_{ab} \frac{\rho_0^{2(1+\tau_{mv})}}{2^{\varepsilon+1}} = \frac{(A_p^m A_s^v)^2}{\rho_0^2 2^{\varepsilon+1}}$. Then, Eq. (43) becomes

$$D_{ab} = \frac{(A_p^m A_s^v)^2}{\rho_0^2} \tilde{D}_{ab} \quad (45)$$

where

$$\tilde{D}_{ab} = \sum_{i=0}^p \sum_{j=0}^p \sum_{k=0}^s \sum_{l=0}^s b_i(p, m) b_j(p, m) b_k(s, v) b_l(s, v) \frac{\varepsilon!}{2^{\varepsilon+1}} \quad (46)$$

⁵Since employing vector modes, it is enough to account for one mode per LP group, where an LP group consists of either 2 modes (for the LP_{0x} modes (with $x \in \{1, 2, \dots\}$)), or 4 modes. Indeed, D_{ab} depends only on the norm of the modes, which is the same for all vector modes within the same LP mode group (while this is not the case for the LP modes of a certain LP mode group). Hence, the later symbolic calculations are speeded up. Note that when only one vector mode per LP mode is employed, a suitable scaling factor within the summation of (38) is needed.

Inserting Eq. (45) in Eq. (38), we obtain

$$\kappa_{\alpha\beta} = \frac{4\pi}{3} \frac{1}{(2N_\alpha + \delta_{\alpha\beta}) N_b} \sum_{a \in I_\alpha} \sum_{b \in I_\beta} (A_p^m A_s^v)^2 \tilde{D}_{ab} \quad (47)$$

where we used $\mathcal{A}_{11} = 2\pi\rho_0^2$ [65].

Notice from Eq. (47) that $\kappa_{\alpha\beta}$ does not depend on R or Δ , but just on the number of modes, and it is expressed only in terms of ratios of integers. Hence, $\kappa_{\alpha\beta}$ can be computed exactly (within the infinite parabolic approximation) with, e.g., the help of a software with symbolic computation capabilities, like MATLAB, as we did. To know which set of modal indices I_α corresponds to a certain mode group, the approach in [43] is helpful. The code we wrote to carry out the symbolic calculations for Eq. (47) has been uploaded to [47]. The analytic values of κ in the SCR for up to 32 mode groups are reported in Table II. For the WCR the analytic values are reported in Table III for up to 10 mode groups (110 modes), and in [47] for up to 32 mode groups (1056 modes).

APPENDIX D

INTERMODAL EFFECTIVE AREA FOR VECTOR MODES

In this section we prove the claim made in Appendix C that Eq. (6) holds not only for the LP modal basis as per [19], but for vector modes 35-37 as well. For a basis of real modes in the weakly guiding regime, like the vector modal basis, the nonlinear coupling coefficients $\gamma^{\kappa_{ab}}$ can be computed as [19, Eq. 55]

$$\gamma^{\kappa_{\alpha\beta}} = \frac{\omega_0 n_2}{c Z_0^2} \frac{1}{(M_\alpha + \delta_{\alpha\beta}) M_\beta} \sum_{a \in I_\alpha} \sum_{b \in I_\beta} \frac{n_{\text{eff}}^2}{N_a^2 N_b^2} I_{ab} \quad (48)$$

where

$$I_{ab} = \frac{1}{6} \int_{-\infty}^\infty \int_{-\infty}^\infty (\|\mathbf{F}_a\|^2 \|\mathbf{F}_b\|^2 + 2\|\mathbf{F}_a \cdot \mathbf{F}_b\|^2) dx dy \quad (49)$$

Consider the two modes \mathbf{F}_a and $\mathbf{F}_{a'}$ with same spatial profile $\|\mathbf{F}_a\| = \|\mathbf{F}_{a'}\|$ and orthogonal polarizations, i.e., $\mathbf{p}_a(\varphi) \cdot \mathbf{p}_{a'}(\varphi) = 0$, and similarly for the modes \mathbf{F}_b and $\mathbf{F}_{b'}$. Such two pair of modes can always be found for the vector modal basis by its definition 35-37. A necessary and sufficient condition to obtain Eq. (6) from Eq. (48) (besides the scaling factor γ) is [19, Eq. 57]

$$I_{ab} + I_{a'b} + I_{ab'} + I_{a'b'} = \frac{4}{3} \int_{-\infty}^\infty \int_{-\infty}^\infty \|\mathbf{F}_a\|^2 \|\mathbf{F}_b\|^2 dx dy \quad (50)$$

To prove that Eq. (50) holds, let us define

$$I_{1,ab} = \int_{-\infty}^\infty \int_{-\infty}^\infty \|\mathbf{F}_a\|^2 \|\mathbf{F}_b\|^2 dx dy \quad (51)$$

and

$$I_{2,ab} = \int_{-\infty}^\infty \int_{-\infty}^\infty \|\mathbf{F}_a \cdot \mathbf{F}_b\|^2 dx dy \quad (52)$$

Firstly, given that by assumption $\|\mathbf{F}_a\| = \|\mathbf{F}_{a'}\|$ and $\|\mathbf{F}_b\| = \|\mathbf{F}_{b'}\|$, we have that

$$I_{1,ab} = I_{1,a'b} = I_{1,ab'} = I_{1,a'b'} \quad (53)$$

Given the separability of the radial and the azimuth dependence, i.e., the radial dependence can be factored out from the previous

integrals, in the following we focus only on the azimuth dependence. We also make use of the fact that a polarization vector has unit norm by definition, i.e., $\|\mathbf{p}_i\| = 1$.

Concerning $I_{2,ab}$, remember that $\mathbf{p}_a \cdot \mathbf{p}_b = \|\mathbf{p}_a\| \|\mathbf{p}_b\| \cos(\vartheta) = \cos(\vartheta)$, with ϑ being the angle between \mathbf{p}_a and \mathbf{p}_b . Since $\mathbf{p}_{a'}$ is orthogonal to \mathbf{p}_a , the angle between $\mathbf{p}_{a'}$ and \mathbf{p}_b is $\pi/2 - \vartheta$. Hence, $\mathbf{p}_{a'} \cdot \mathbf{p}_b = \sin(\vartheta)$. Given that $\int_0^{2\pi} \sin^2(\vartheta) d\varphi = \int_0^{2\pi} \cos^2(\vartheta) d\varphi = \pi$, it follows that $I_{2,ab} = I_{2,a'b}$. Additionally, due to the orthogonality between \mathbf{p}_a and $\mathbf{p}_{a'}$, and between \mathbf{p}_b and $\mathbf{p}_{b'}$, it follows that $I_{2,ab} = I_{2,a'b'}$ and $I_{2,a'b} = I_{2,ab'}$. Hence,

$$I_{2,ab} = I_{2,a'b} = I_{2,ab'} = I_{2,a'b'} \quad (54)$$

Note also that

$$I_{2,ab} \propto \int_0^{2\pi} \|\mathbf{p}_a(\varphi) \cdot \mathbf{p}_b(\varphi)\|^2 d\varphi = \int_0^{2\pi} \cos^2(\vartheta) d\varphi = \pi$$

and

$$I_{1,ab} \propto \int_0^{2\pi} \|\mathbf{p}_a(\varphi)\|^2 \|\mathbf{p}_b(\varphi)\|^2 d\varphi = 2\pi$$

Thus,

$$I_{2,ab} = I_{1,ab}/2 \quad (55)$$

Hence, plugging Eq. (53) and Eq. (54) into the left-hand side of Eq. (50), and using Eq. (55), we get $I_{ab} + I_{a'b} + I_{ab'} + I_{a'b'} = 4/6 I_{1,ab} + 8/6 I_{2,ab} = 4/6 I_{1,ab} + 4/6 I_{1,ab} = 4/3 I_{1,ab}$, which proves Eq. (50).

APPENDIX E

NONLINEARITY COEFFICIENTS OF STEP-INDEX FIBERS

The derivation of closed-form expressions for the nonlinear coupling coefficients in SIMMFs has few differences compared to GIMMFs. Firstly, the dependence of γ on R and on Δ is not the same as for GIMMFs. This is because for a SIMMF, instead of Eq. (23), the fitted relation for the spot-size of the Gaussian approximation is [69, Eq. 8]

$$\frac{r_0}{R} = A + \frac{B}{V^{1.5}} + \frac{C}{V^6} \quad (56)$$

where $A = 0.65$, $B = 1.619$, $C = 2.879$, and we have verified the last term to be negligible in our case. The variational approach formula for a SIMMF yields [44, Table 15-2]

$$\frac{r_0}{R} \propto \frac{1}{\sqrt{\log V}} \quad (57)$$

which, however, we have verified to be less accurate than Eq. (56). Hence, when R is varied fixed Δ , with the help of Eqs. (22), (56) and (11) it is found that

$$\mathcal{A}_{11} \approx \pi \left(\frac{A}{\text{NA}k_0} \right)^2 2M \left(A + \frac{B}{(2M)^{0.75}} \right)^2 \quad (58)$$

If Δ is varied, while keeping R fixed, then

$$\mathcal{A}_{11} \approx \pi R^2 \left(A + \frac{B}{(2M)^{0.75}} \right)^2 \quad (59)$$

As a side note, \mathcal{A}_{11} increases slower than in a GIMMF when R is fixed, and decreases slower when Δ is fixed, due to the different relations between r_0 and V .

We observed the numerical results to agree well with the theoretical scaling laws $M \left(A + \frac{B}{(2M)^{0.75}} \right)^2$ and $\left(A + \frac{B}{(2M)^{0.75}} \right)^2$, see Fig.10, but for slightly different proportionality factors than $\pi \left(\frac{A}{\text{NA}k_0} \right)^2 2$ and πR^2 .

The dependence of κ on M is numerically found to be essentially constant (thus weaker than $1/\sqrt{M}$ for GIMMFs), see Fig.11, even though we did not provide an analytic derivation of κ as for GIMMFs. Ideally, it would be possible to consider the weakly guiding analytic expressions for the modal profiles of SIMMFs, which depend on Bessel functions [44, Table 14-6], and follow a procedure analogous to the one for GIMMFs in Appendix C. For this purpose, formulas for integrals involving squares of Bessels functions (and their products) given in [70, p. 431] and in [71, Eq. 14] could be useful.

APPENDIX F

NONLINEARITY COEFFICIENT FOR NON-PARABOLIC GRADED INDEX FIBERS

The deviations in $\gamma\kappa$ in case of non-parabolic GIMMFs could be ideally studied with a similar approach to the one in Section IV. That is, by independently approximating γ (or, equivalently, \mathcal{A}_{11}) and κ . Strictly speaking, it would be necessary to recompute also the cutoff frequencies and, hence, a substitute relation for Eq. (10). However, given the grading exponent $g = 2 + \delta$, with $\delta \in [-10\%, +10\%]$ (conservative realistic range [34]), it can be safely assumed that Eq. (10) is almost untouched.

Concerning κ , an analytic derivation in the sense of Appendix C would be quite involved because of the non-trivial expressions of the modal profiles. Extensive computations with the numerical method could be carried out to fit a relation similar to Eq. (17) which relates κ_{ab} to M . However, we do not expect significant changes in view of a little δ , as confirmed by Fig. 12, for which we verified that the values of κ numerically computed for fibers in the literature (which in general do not have a parabolic graded index) are close to the ones of parabolic GIMMFs.

For \mathcal{A}_{11} , it is possible to exploit the Gaussian approximation for a generic GI profile [64, Eq. 11]. Then, with the same procedure as in Appendices A and B, for a generic power-law GI profile with grading exponent $g = 2 + \delta$, neglecting the last two terms of the Gaussian approximation for r_0/R [64, Eq. 11], it holds

$$\gamma\kappa(\delta) \approx \frac{n_2\omega_0}{c} \frac{7}{2\pi R^2} \frac{V^{-\frac{\delta}{4+\delta}}}{\bar{A}^2} \quad (60)$$

where $\bar{A} = \left(\frac{2}{5} \left(1 + 4 \left(\frac{2}{2+\delta} \right)^{5/6} \right) \right)^{0.5}$.

Then, the ratio between $\gamma\kappa$ of Eq. (60) and the parabolic case of Eq. (16) is given by

$$\varepsilon = \frac{\gamma\kappa(\delta)}{\gamma\kappa(\delta=0)} = V^{-\frac{\delta}{4+\delta}} \frac{2}{\bar{A}^2} \quad (61)$$

For $V \in [1, 100]$, which covers the whole range of Fig.12, and $\delta \in [-10\%, +10\%]$, it has been numerically observed that the maximum excursion of ε is $\pm 10\%$.

ACKNOWLEDGMENTS

The authors acknowledge fruitful discussions with Paolo Serena of the University of Parma.

REFERENCES

- [1] P. Sillard, K. Benyahya, D. Soma, G. Labroille, P. Jian, K. Igarashi, R. Ryf, N. K. Fontaine, G. Rademacher, and K. Shibahara, "Few-mode fiber technology, deployments, and systems," *Proceedings of the IEEE*, vol. 110, no. 11, pp. 1804–1820, 2022.
- [2] T. Matsui, P. L. Pondillo, and K. Nakajima, "Weakly coupled multicore fiber technology, deployment, and systems," *Proceedings of the IEEE*, vol. 110, no. 11, pp. 1772–1785, 2022.
- [3] T. Hayashi, T. Sakamoto, Y. Yamada, R. Ryf, R.-J. Essiambre, N. Fontaine, M. Mazur, H. Chen, and T. Hasegawa, "Randomly-coupled multi-core fiber technology," *Proceedings of the IEEE*, vol. 110, no. 11, pp. 1786–1803, 2022.
- [4] D. Askarov and J. M. Kahn, "Long-period fiber gratings for mode coupling in mode-division-multiplexing systems," *Journal of Lightwave Technology*, vol. 33, no. 19, pp. 4032–4038, 2015.
- [5] S. Ö. Arık, K.-P. Ho, and J. M. Kahn, "Group delay management and multiinput multioutput signal processing in mode-division multiplexing systems," *Journal of Lightwave Technology*, vol. 34, no. 11, pp. 2867–2880, 2016.
- [6] H. Liu, H. Wen, B. Huang, R. A. Correa, P. Sillard, H. Chen, Z. Li, and G. Li, "Reducing group delay spread using uniform long-period gratings," *Scientific reports*, vol. 8, no. 1, p. 3882, 2018.
- [7] K.-P. Ho and J. M. Kahn, "Chapter 11 - mode coupling and its impact on spatially multiplexed systems," in *Optical Fiber Telecommunications (Sixth Edition)*, sixth edition ed., ser. Optics and Photonics, I. P. Kaminow, T. Li, and A. E. Willner, Eds. Boston: Academic Press, 2013, pp. 491–568. [Online]. Available: <https://www.sciencedirect.com/science/article/pii/B9780123969606000110>
- [8] C. Antonelli, A. Mecozzi, and M. Shtaif, "The delay spread in fibers for sdm transmission: dependence on fiber parameters and perturbations," *Opt. Express*, vol. 23, no. 3, pp. 2196–2202, Feb 2015. [Online]. Available: <https://opg.optica.org/oe/abstract.cfm?URI=oe-23-3-2196>
- [9] S. Ö. Arık, K.-P. Ho, and J. M. Kahn, "Delay spread reduction in mode-division multiplexing: Mode coupling versus delay compensation," *Journal of Lightwave Technology*, vol. 33, no. 21, pp. 4504–4512, 2015.
- [10] B. J. Puttnam, G. Rademacher, and R. S. Luís, "Space-division multiplexing for optical fiber communications," *Optica*, vol. 8, no. 9, pp. 1186–1203, Sep 2021. [Online]. Available: <https://opg.optica.org/optica/abstract.cfm?URI=optica-8-9-1186>
- [11] B. Huang, N. K. Fontaine, H. Chen, J. Cang, R. Ryf, R.-J. Essiambre, T. Nagashima, T. Sasaki, and T. Hayashi, "Minimizing the modal delay spread in coupled-core two-core fiber," in *2016 Conference on Lasers and Electro-Optics (CLEO)*, 2016, pp. 1–2.
- [12] G. Rademacher, R. S. Luís, B. J. Puttnam, R. Ryf, S. van der Heide, T. A. Eriksson, N. K. Fontaine, H. Chen, R.-J. Essiambre, Y. Awaji *et al.*, "A comparative study of few-mode fiber and coupled-core multi-core fiber transmission," *Journal of Lightwave Technology*, vol. 40, no. 6, pp. 1590–1596, 2022.
- [13] F. M. Ferreira and F. A. Barbosa, "Maximizing the capacity of graded-index multimode fibers in the linear regime," *Journal of Lightwave Technology*, vol. 42, no. 5, pp. 1626–1633, 2024.
- [14] P. Sillard, M. Bigot, K. de Jongh, F. Achten, G. Rademacher, R. Luís, and B. Puttnam, "55-spatial-mode fiber for space division multiplexing," in *2023 Optical Fiber Communications Conference and Exhibition (OFC)*. IEEE, 2023, pp. 1–3.
- [15] L. Palmieri and A. Galtarossa, "Intramodal dispersion properties of step-index few-mode spun fibers," *Journal of Lightwave Technology*, vol. 34, no. 2, pp. 303–313, 2016.
- [16] G. Di Sciuillo, M. van den Hout, G. Rademacher, R. S. Luís, B. J. Puttnam, N. K. Fontaine, R. Ryf, C. Haoshuo, M. Mazur, D. T. Neilson, P. Sillard, F. Achten, J. Sakaguchi, C. Okonkwo, A. Mecozzi, C. Antonelli, and H. Furukawa, "Reduction of modal dispersion in a long-haul 15-mode fiber link by means of mode permutation," in *2023 European Conference on Optical Communications (ECOC)*, 2023, pp. 250–253(3). [Online]. Available: <https://digital-library.theiet.org/content/conferences/10.1049/icp.2023.2052>
- [17] G. Rademacher, R. S. Luís, B. J. Puttnam, N. K. Fontaine, M. Mazur, H. Chen, H. Chen, R. Ryf, D. T. Neilson, D. Dahl, J. Carpenter, P. Sillard, F. Achten, M. Bigot, J. Sakaguchi, and H. Furukawa, "3.56 peta-bit/s c+1 band transmission over a 55-mode multi-mode fiber," in *2023 European Conference on Optical Communications (ECOC)*, 2023, pp. 9–12(3). [Online]. Available: <https://digital-library.theiet.org/content/conferences/10.1049/icp.2023.1834>
- [18] P. J. Winzer and D. T. Neilson, "From scaling disparities to integrated parallelism: A decathlon for a decade," *Journal of Lightwave Technology*, vol. 35, no. 5, pp. 1099–1115, 2017.
- [19] C. Antonelli, M. Shtaif, and A. Mecozzi, "Modeling of nonlinear propagation in space-division multiplexed fiber-optic transmission," *Journal of Lightwave Technology*, vol. 34, no. 1, pp. 36–54, 2016.
- [20] P. Carniello, F. M. Ferreira, and H. Norbert, "Scaling of the nonlinear coupling coefficient in multimode fibers," in *2023 European Conference on Optical Communications (ECOC)*, 2023, pp. 1394–1397(3). [Online]. Available: <https://digital-library.theiet.org/content/conferences/10.1049/icp.2023.2554>
- [21] P. Serena, C. Lasagni, A. Bononi, C. Antonelli, and A. Mecozzi, "The ergodic gn model for space-division multiplexing with strong mode coupling," *Journal of Lightwave Technology*, 2022.
- [22] C. Lasagni, P. Serena, A. Bononi, A. Mecozzi, and C. Antonelli, "Impact of mode dispersion on cross-phase modulation in few-mode fiber transmissions," in *2023 European Conference on Optical Communications (ECOC)*, 2023, pp. 1242–1245(3). [Online]. Available: <https://digital-library.theiet.org/content/conferences/10.1049/icp.2023.2516>
- [23] F. J. Garcia-Gomez and G. Kramer, "Rate and power scaling of space-division multiplexing via nonlinear perturbation," *Journal of Lightwave Technology*, vol. 40, no. 15, pp. 5077–5082, 2022.
- [24] A. Mecozzi, C. Antonelli, and M. Shtaif, "Nonlinear propagation in multi-mode fibers in the strong coupling regime," *Optics express*, vol. 20, no. 11, pp. 11 673–11 678, 2012.
- [25] S. Mumtaz, R.-J. Essiambre, and G. P. Agrawal, "Nonlinear propagation in multimode and multicore fibers: Generalization of the manakov equations," *Journal of Lightwave Technology*, vol. 31, no. 3, pp. 398–406, 2013.
- [26] D. Gloge, "Weakly guiding fibers," *Applied optics*, vol. 10, no. 10, pp. 2252–2258, 1971.
- [27] A. Mecozzi, C. Antonelli, and M. Shtaif, "Coupled manakov equations in multimode fibers with strongly coupled groups of modes," *Optics express*, vol. 20, no. 21, pp. 23 436–23 441, 2012.
- [28] G. P. Agrawal, *Fiber-Optic Communication Systems*. John Wiley & Sons, 2021.
- [29] F. M. Ferreira, C. S. Costa, S. Sygletos, and A. D. Ellis, "Semi-analytical modelling of linear mode coupling in few-mode fibers," *Journal of Lightwave Technology*, vol. 35, no. 18, pp. 4011–4022, 2017.
- [30] —, "Nonlinear performance of few-mode fiber links with intermediate coupling," *Journal of Lightwave Technology*, vol. 37, no. 3, pp. 989–999, 2019.
- [31] S. Buch, S. Mumtaz, R.-J. Essiambre, A. M. Tulino, and G. P. Agrawal, "Averaged nonlinear equations for multimode fibers valid in all regimes of random linear coupling," *Optical Fiber Technology*, vol. 48, pp. 123–127, 2019.
- [32] G. Keiser, *Optical Fiber Communications, Fourth Edition*. McGraw-Hill, 2011.
- [33] P. Sillard, M. Bigot-Astruc, and D. Molin, "Few-mode fibers for mode-division-multiplexed systems," *Journal of Lightwave Technology*, vol. 32, no. 16, pp. 2824–2829, 2014.
- [34] F. M. Ferreira, D. Fonseca, and H. J. A. da Silva, "Design of few-mode fibers with m-modes and low differential mode delay," *Journal of Lightwave Technology*, vol. 32, no. 3, pp. 353–360, 2014.
- [35] P. Sillard, D. Molin, M. Bigot-Astruc, K. De Jongh, F. Achten, J. E. Antonio-López, and R. Amezcua-Correa, "Micro-bend-resistant low-differential-mode-group-delay few-mode fibers," *Journal of Lightwave Technology*, vol. 35, no. 4, pp. 734–740, 2017.
- [36] P. Carniello, "Is the weak coupling nonlinear sdm channel worse than the strong coupling one?" in *2024 24rd International Conference on Transparent Optical Networks (ICTON)*, 2024.
- [37] W. Hermann and D. U. Wiechert, "Refractive index of doped and undoped pcvd bulk silica," *Materials research bulletin*, vol. 24, no. 9, pp. 1083–1097, 1989.
- [38] S. Ö. Arık, D. Askarov, and J. M. Kahn, "Adaptive frequency-domain equalization in mode-division multiplexing systems," *Journal of Lightwave Technology*, vol. 32, no. 10, pp. 1841–1852, 2014.
- [39] K. T. Kernetzky, "Numerical optimization of ultra-broadband wavelength conversion in nonlinear optical waveguides," Ph.D. dissertation,

- Technische Universität München, 2023. [Online]. Available: <https://mediatum.ub.tum.de/1687894>
- [40] K. Kawano and T. Kitoh, *Introduction to Optical Waveguide Analysis: Solving Maxwell's Equation and the Schrödinger Equation*. John Wiley & Sons, 2004.
- [41] F. Schmidt and K. Petermann, "Investigation of lp- and vector-modes for the analysis of space-division multiplexed systems in the nonlinear regime," *Journal of Lightwave Technology*, vol. 35, no. 22, pp. 4859–4864, 2017.
- [42] C. Antonelli, A. Mecozzi, M. Shtaif, and P. J. Winzer, "Nonlinear propagation equations in fibers with multiple modes—transitions between representation bases," *Appl Photonics*, vol. 4, no. 2, p. 022806, 2019.
- [43] T. I. Lukowski and F. P. Kapron, "Parabolic fiber cutoffs: A comparison of theories," *J. Opt. Soc. Am.*, vol. 67, no. 9, pp. 1185–1187, Sep 1977. [Online]. Available: <https://opg.optica.org/abstract.cfm?URI=josa-67-9-1185>
- [44] A. W. Snyder and J. D. Love, *Optical Waveguide Theory*. Chapman and Hall, 1983.
- [45] "Corning smf-28e+ optical fiber." Corning Incorporated, November 2021. [Online]. Available: https://www.corning.com/media/worldwide/coc/documents/Fiber/product-information-sheets/PI1463_07-14_English.pdf
- [46] R. Ryf and C. Antonelli, "Space-division multiplexing," *Springer Handbook of Optical Networks*, pp. 353–393, 2020.
- [47] P. Carniello and F. M. Ferreira, "Dataset of numerical and analytical nonlinearity coefficients of multimode fibers," 2024. [Online]. Available: <https://mediatum.ub.tum.de/1752664>
- [48] M.-J. Li, B. Hoover, S. Li, S. Bickham, S. Ten, E. Ip, Y.-K. Huang, E. Mateo, Y. Shao, and T. Wang, "Low delay and large effective area few-mode fibers for mode-division multiplexing," in *2012 17th Opto-Electronics and Communications Conference*. IEEE, 2012, pp. 495–496.
- [49] K. Sato, R. Maruyama, N. Kuwaki, S. Matsuo, and M. Ohashi, "Optimized graded index two-mode optical fiber with low dmd, large a eff and low bending loss," *Optics express*, vol. 21, no. 14, pp. 16 231–16 238, 2013.
- [50] R. Ryf, N. K. Fontaine, H. Chen, B. Guan, S. Randel, N. Sauer, S. B. Yoo, A. Koonen, R. Delbue, P. Pupalaiakis *et al.*, "23 tbit/s transmission over 17-km conventional 50- μ m graded-index multimode fiber," in *Optical Fiber Communication Conference*. Optica Publishing Group, 2014, pp. Th5B–1.
- [51] T. Mori, T. Sakamoto, M. Wada, T. Yamamoto, and F. Yamamoto, "Few-mode fibers supporting more than two lp modes for mode-division-multiplexed transmission with mimo dsp," *Journal of Lightwave Technology*, vol. 32, no. 14, pp. 2468–2479, 2014.
- [52] P. Sillard, D. Molin, M. Bigot-Astruc, K. De Jongh, F. Achten, A. M. Velázquez-Benítez, R. Amezcua-Correa, and C. M. Okonkwo, "Low-differential-mode-group-delay 9-lp-mode fiber," *Journal of Lightwave Technology*, vol. 34, no. 2, pp. 425–430, 2016.
- [53] P. Sillard, D. Molin, M. Bigot-Astruc, A. Amezcua-Correa, K. de Jongh, and F. Achten, "50 μ m multimode fibers for mode division multiplexing," *Journal of Lightwave Technology*, vol. 34, no. 8, pp. 1672–1677, 2016.
- [54] P. Sillard, D. Molin, M. Bigot-Astruc, K. de Jongh, and F. Achten, "Rescaled multimode fibers for mode-division multiplexing," *Journal of Lightwave Technology*, vol. 35, no. 8, pp. 1444–1449, 2017.
- [55] C. Antonelli, A. Mecozzi, and M. Shtaif, "Scaling of inter-channel nonlinear interference noise and capacity with the number of strongly coupled modes in sdm systems," in *2016 Optical Fiber Communications Conference and Exhibition (OFC)*, 2016, pp. 1–3.
- [56] M. Shtaif, C. Antonelli, A. Mecozzi, and X. Chen, "Challenges in estimating the information capacity of the fiber-optic channel," *Proceedings of the IEEE*, vol. 110, no. 11, pp. 1655–1678, 2022.
- [57] C. Lasagni, P. Serena, A. Bononi, A. Mecozzi, and C. Antonelli, "Effect of modal dispersion on the nonlinear interference noise in sdm transmissions," in *2024 Optical Fiber Communications Conference and Exhibition (OFC)*, 2024, pp. 1–3.
- [58] F. A. Barbosa and F. M. Ferreira, "On a scalable path for multimode sdm transmission," *Journal of Lightwave Technology*, vol. 42, no. 1, pp. 219–228, 2024.
- [59] G. Rademacher and K. Petermann, "Nonlinear gaussian noise model for multimode fibers with space-division multiplexing," *Journal of Lightwave Technology*, vol. 34, no. 9, pp. 2280–2287, 2016.
- [60] D. Marcuse, *Theory of Dielectric Optical Waveguides*, ser. Quantum electronics—principles and applications. Academic Press Inc, 1974.
- [61] L. Palmieri and A. Galtarossa, "Coupling effects among degenerate modes in multimode optical fibers," *IEEE Photonics Journal*, vol. 6, no. 6, pp. 1–8, 2014.
- [62] A. B. Fallahkhair, K. S. Li, and T. E. Murphy, "Vector finite difference modesolver for anisotropic dielectric waveguides," *Journal of Lightwave Technology*, vol. 26, no. 11, pp. 1423–1431, 2008.
- [63] M. Hashimoto, "Cutoff frequencies of vector wave modes in cladded inhomogeneous optical fibre," *Electronics Letters*, vol. 21, no. 16, pp. 806–808, 1980.
- [64] D. Marcuse, "Gaussian approximation of the fundamental modes of graded-index fibers," *J. Opt. Soc. Am.*, vol. 68, no. 1, pp. 103–109, Jan 1978. [Online]. Available: <https://opg.optica.org/abstract.cfm?URI=josa-68-1-103>
- [65] A. Mafi, "Pulse propagation in a short nonlinear graded-index multimode optical fiber," *Journal of Lightwave Technology*, vol. 30, no. 17, pp. 2803–2811, 2012.
- [66] G. B. Arfken, H. J. Weber, and F. E. Harris, *Mathematical methods for physicists: a comprehensive guide*. Academic press, 2011.
- [67] Y. Jiang, G. Ren, W. Jin, Y. Xu, W. Jian, and S. Jian, "Polarization properties of fiber-based orbital angular momentum modes," *Optical Fiber Technology*, vol. 38, pp. 113–118, 2017.
- [68] J. Miller, "Formulas for integrals of products of associated legendre or laguerre functions," *Mathematics of Computation*, vol. 17, no. 81, pp. 84–87, 1963.
- [69] D. Marcuse, "Loss analysis of single-mode fiber splices," *The Bell System Technical Journal*, vol. 56, no. 5, pp. 703–718, 1977.
- [70] W. Rosenheinrich, "Tables of some indefinite integrals of bessel functions," *University of Applied Sciences, Germany*, 2022. [Online]. Available: https://www.eah-jena.de/fileadmin/user_upload/eah-jena.de/fachbereich/gw/Ehemalige/rosenheinrich/besint.pdf
- [71] E. Matagne, "Some integrals involving squares of bessel functions and generalized legendre polynomials," *Advanced Electromagnetics*, vol. 11, no. 4, pp. 80–83, 2022.



Paolo Carniello received the B.S. degree from the University of Udine, Italy, in electronic engineering in 2019, and the M.S. degree from Politecnico di Torino, Italy, in telecommunications engineering in 2021. He is currently working towards the Ph.D. degree at the Technical University of Munich, Germany. His research interests focus on space-division multiplexing for optical communications systems: channel modeling, signal processing, and aspects of applied information theory.



Filipe Ferreira is a Principal Research Fellow and UKRI Future Leaders Fellow in the Department of Electronic and Electrical Engineering at University College London. His research focuses on exploring massive spatial parallelism in optical fibres by integrating spatial light modulation with machine learning. Filipe also serves as the Chair of the IEEE UK & Ireland Photonics Society Chapter, contributing to the advancement of the photonics community. He earned his PhD in Electrical and Computer Engineering from the University of Coimbra in 2014, specializing in high-capacity optical transmission in multipath fibres to surpass the limits of conventional single-mode systems. During his doctoral studies, Filipe worked as a research engineer at Nokia Siemens Networks, where he led advancements in mode-division multiplexing as part of the EU-FP7 project MODEGAP. Subsequently, he was awarded a prestigious Marie Skłodowska-Curie Fellowship to continue his research at Aston University, where he made significant contributions to understanding the interplay between linear and nonlinear impairments in multi-mode fibres and their impact on transmission capacity. In 2020, Filipe began his UKRI Future Leaders Fellowship at UCL, focusing on high-capacity optical fibre transmission, spatially multiplexed systems, digital nonlinear compensation, and advanced optical fibre design. He has co-authored over 140 peer-reviewed journal and conference papers, including numerous invited contributions, and delivered more than 30 invited talks at major international events such as ECOC and OFC. He is also the lead inventor on four active WO patents.



Norbert Hanik received the Dipl.-Ing. degree in electrical engineering (with a thesis on Digital Spread Spectrum Systems) and the Dr.-Ing. degree (with a dissertation on nonlinear effects in optical signal transmission) from the Munich University of Technology, Munich, Germany, in 1989 and 1995, respectively. He was a Research Associate at the Institute for Telecommunications, Technical University of Munich, from 1989 to 1995, where he worked in the area of Optical Communications. From 1995 to 2004 he has been with the Technology Center

of Deutsche Telekom, Berlin, heading the research group System Concepts of Photonic Networks. During his work there, he contributed to a multitude of national, international, and Telekom internal R&D-projects. From January to March 2002, he was a Visiting Professor at Research Center COM, Technical University of Denmark, Lyngby. Since 2004 he holds the Professorship for Line Transmission Technology at the Technical University of Munich. His primary research interests are in the fields of design and optimization of optical communication systems.